



**Politecnico  
di Torino**



UNIVERSITY OF  
**OXFORD**

Department of Mechanical and Aerospace Engineering

Master's degree programme in:

**AUTOMOTIVE ENGINEERING**

# Thermal Management Strategy for a Formula Student Vehicle

## Modelling and Control of the Cooling Loop

Supervisors:

Prof. D'Ambrosio Stefano

Dr. Walker Ryan

Candidate:

De Simone Eugenio

March 2025



# Contents

List of Figures	IV
Abstract	VII
<b>1 Introduction</b>	<b>1</b>
<b>2 Thermal Model</b>	<b>6</b>
2.1 Cooling Loop . . . . .	6
2.2 Driving Cycle . . . . .	8
2.3 Electric Motor and Inverter Power Evaluation . . . . .	12
2.4 Fan . . . . .	13
2.4.1 Fan Control Unit . . . . .	15
2.4.2 Thermodynamic Variables . . . . .	17
2.5 Radiator . . . . .	18
2.6 Pumps . . . . .	22
2.6.1 Pumps Control Unit . . . . .	26
2.7 Inverter Cold Plate . . . . .	26
2.8 Hose . . . . .	30
2.9 Electric Motor Cooling Jacket . . . . .	31
2.10 Catch Can . . . . .	34

<b>3</b>	<b>Simulations</b>	<b>36</b>
3.1	Sensitivity Analysis . . . . .	36
3.1.1	Ambient Temperature Analysis . . . . .	37
3.1.2	Inverter Efficiency Settings Analysis . . . . .	38
3.1.3	Fan Control Settings Analysis . . . . .	39
3.1.4	Pump Control Settings Analysis . . . . .	43
3.2	Full Power Configuration . . . . .	46
3.2.1	Temperature Analysis . . . . .	46
3.2.2	Energy Consumption . . . . .	48
<b>4</b>	<b>Control Strategy</b>	<b>52</b>
4.1	Reference Temperatures . . . . .	53
4.2	PID . . . . .	54
4.2.1	Implementation . . . . .	54
4.2.2	Tuning . . . . .	55
4.2.3	Outcomes . . . . .	57
4.3	MPC . . . . .	60
4.3.1	Implementation . . . . .	62
4.3.2	Tuning . . . . .	63
4.3.3	Outcomes . . . . .	63
<b>5</b>	<b>Conclusions</b>	<b>69</b>
	<b>Bibliography</b>	<b>72</b>

# List of Figures

1.1	Formula Student event in Germany . . . . .	1
1.2	Oxford University Racing team . . . . .	3
1.3	Radiator detail . . . . .	4
2.1	Model overview . . . . .	7
2.2	Vehicle setup before the test . . . . .	8
2.3	Vehicle speed plot . . . . .	9
2.4	EM speed plot . . . . .	10
2.5	EM torque plot . . . . .	10
2.6	Driving cycle block . . . . .	11
2.7	EM power block overview . . . . .	12
2.8	San Ace 140 DC fan . . . . .	14
2.9	Fan block overview . . . . .	15
2.10	Fan control logic . . . . .	16
2.11	Air thermodynamic variables block . . . . .	17
2.12	Davies Craig EBP15 DC pump . . . . .	22
2.13	Pumps block . . . . .	24
2.14	Pumps coolant fluid dynamics modeling . . . . .	24
2.15	Pumps control unit . . . . .	26
2.16	Inverter cold plate . . . . .	27

2.17	Inverter block . . . . .	28
2.18	Inverter cold plate internal view . . . . .	29
2.19	Hose block . . . . .	30
2.20	Plettenburg Nova-15 permanent magnet synchronous motors (PMSMs)	31
2.21	EM block overview . . . . .	32
2.22	EM test rig . . . . .	33
2.23	Catch can model . . . . .	34
3.1	Variation of EM outlet temperature as a function of ambient tem- perature . . . . .	38
3.2	Variation of coldplate outlet temperature as a function of inverter efficiency . . . . .	39
3.3	Variation of EM outlet temperature as a function of fan control settings . . . . .	40
3.4	Variation of $\Delta$ temperature across the EM cooling jacket as a func- tion of fan control settings . . . . .	41
3.5	Variation of PM outlet temperature as a function of fan control settings . . . . .	42
3.6	Variation of $\Delta$ temperature across the PM cooling plate as a func- tion of fan control settings . . . . .	42
3.7	Variation of EM cooling jacket outlet temperature as a function of pumps control settings . . . . .	44
3.8	Variation of $\Delta$ temperature across the EM cooling jacket as a func- tion of pump control settings . . . . .	44
3.9	Variation of PM cold plate outlet temperature as a function of pumps control settings . . . . .	45
3.10	Variation of $\Delta$ temperature across the PM cold plate as a function of pump control settings . . . . .	45

3.11	Motor cooling jacket outlet temperature in full power configuration	47
3.12	Inverter cold plate outlet temperature in full power configuration	47
3.13	Fan energy consumption in full power configuration . . . . .	49
3.14	Pump energy consumption in full power configuration . . . . .	50
3.15	Total energy consumption in full power configuration . . . . .	51
4.1	Block connection using PID controllers . . . . .	55
4.2	Fan PID controller . . . . .	56
4.3	Pump PID controller . . . . .	57
4.4	Temperature in the cooling loop using PID controllers . . . . .	58
4.5	Fan energy consumption using PID controllers . . . . .	59
4.6	Pumps energy consumption using PID controllers . . . . .	59
4.7	Total energy consumption using PID controllers . . . . .	60
4.8	Block connection using MPC controller . . . . .	62
4.9	Temperature in the cooling loop using MPC controllers . . . . .	64
4.10	Fan energy consumption using MPC controller . . . . .	65
4.11	Pumps energy consumption using MPC controller . . . . .	66
4.12	Total energy consumption using MPC controller . . . . .	66
4.13	Comparison of energy consumption using different control strategy	67

# Abstract

This thesis aims to develop a thermal management strategy for a Formula Student vehicle, focusing on the control of the cooling system auxiliaries, specifically pumps and fans.

The work is divided into two main stages. First, a thermal model of the existing cooling system is developed in MATLAB Simulink, based on the architecture of the Oxford University Racing 2023 single-seater. The model is then simulated to assess its dynamic behavior and responsiveness. The model's response is tested under varying external and operating conditions. Simulations are conducted to establish a reference condition. A maximum cooling scenario is simulated, where the cooling system auxiliaries operate at full power. This provides a baseline in terms of temperature at critical points of the cooling loop and energy consumption from the low-voltage battery pack.

The second stage focuses on designing a control strategy. The control variables are associated with the radiator fans and pumps. The control strategy aims to maintain the temperature close to a target value while avoiding excessive cooling of components. Two control strategies are presented. The first is based on PID controllers, chosen for their simplicity and ease of implementation in Simulink. However, PID controllers may exhibit overshoot, which must be managed to avoid excessive temperature fluctuations and potential damage to powertrain components. The second approach utilizes a Model Predictive Controller (MPC), which

is better suited for handling MIMO (Multiple Input Multiple Output) dynamic systems and predicting variations. This controller demonstrates greater robustness, but its computational demand is a key consideration for vehicle implementation.

The conclusions show that implementing a control strategy that prevents excessive cooling of powertrain components can result in an energy saving of approximately 60%. This, in turn, brings several benefits, such as a lighter battery pack due to the reduced number of cells, and thus contributing to improved vehicle dynamics and lower costs. Additionally, in the context of Formula Student competitions, it can lead to higher scores in both static and dynamic events. A well-structured thermal management strategy ensures safe operation, preventing overheating and unnecessary energy losses, ultimately enhancing the team's competitive edge.

# Chapter 1

## Introduction

Since its inception, Formula Student has served as a platform for innovation and engineering development. Every year, hundreds of universities compete, striving to introduce new technological advancements while reinforcing an engineering mindset. The essence of a Formula Student team lies in continuous improvement, optimizing performance, and effectively utilizing available resources.



Figure 1.1: Formula Student event in Germany

Formula Student competitions consist of two main categories of events: static

and dynamic. Static events assess engineering design, cost analysis, and business presentation, evaluating the technical and economic feasibility of the vehicle. Dynamic events, on the other hand, test the performance of the car in real-world conditions, including acceleration, skid pad, autocross, endurance, and efficiency trials. Below the score for every event are reported.

**Static Events:**

1. **Engineering Design** – 150 points
2. **Cost and Manufacturing** – 100 points
3. **Business Plan Presentation** – 75 points

**Dynamic Events:**

1. **Acceleration** – 75 points
2. **Skid Pad** – 75 points
3. **Autocross** – 100 points
4. **Efficiency** – 100 points
5. **Endurance** – 325 points

**Total Points: 1000**

This thesis has been conducted in collaboration with the University of Oxford and its Formula Student team, Oxford University Racing (OUR). Additionally, the experience gained through participation in the Formula Student team Squadra Corse of Politecnico di Torino has played a fundamental role in shaping this work.

The 2022 season marked a significant transition for OUR, as the team decided to shift from an internal combustion engine vehicle, designed for the combustion



Figure 1.2: Oxford University Racing team

category, to an electric powertrain (EV). The subsequent years have been characterized by a period of team restructuring to accommodate the challenges and requirements associated with this change in vehicle architecture.

From a cooling perspective, a simple yet oversized architecture was initially selected. This decision was justified by the limited amount of data collected on the cooling system and the necessity to ensure the reliability and longevity of the powertrain. The cooling system consists of two independent and symmetrical circuits located on the right and left sides of the vehicle. For the purposes of this study, only one half of the cooling system will be analyzed.

Each side of the system features a radiator, adopted from the cooling system of the BMW GS 1200 motorcycle. The radiator is positioned within the side pods, adjacent to the driver. In series with the radiator, two brushless Electric Booster Pumps (EBP) with magnetic drive [1] have been installed. The choice of using two pumps in series is motivated by two primary factors: first, the lack of precise knowledge regarding pressure losses within the system; second, the need to

ensure fluid circulation in case of a pump failure. Additionally, the cooling jacket of the rear motor is connected in series with the system. For the purpose of this study, the thermal model will also include the cooling of power modules via a cold plate, a feature planned in the development roadmap but not yet implemented as of 2024. The cold plate will be simulated as part of the cooling loop. The cooling mechanism is based on forced convection, with a San Ace 140 9GV fan [2] installed downstream of the radiator.



Figure 1.3: Radiator detail

The vehicle under study is equipped with two battery packs. The high-voltage (HV) battery pack supplies power to the powertrain, which includes the inverter and electric motor. The low-voltage (LV) battery pack powers all auxiliary and

control systems, including the cooling system. Reducing energy demand for cooling may enable a reduction in the weight of the LV battery pack.

During track testing, the cooling system auxiliaries, including pumps and fans, have been operated at full power. This approach has been adopted due to the absence of experimental data collected under real racing conditions, leading to the decision to oversize the cooling system. The development of a thermal model will facilitate the simulation of the cooling system, laying the groundwork for an optimized control strategy. The implementation of the latter will allow the system to maintain components at a reference temperature, ensuring proper operation while accounting for fluctuations in operating conditions and uncertainties in state measurements. Avoiding excessive cooling will result in energy savings.

A thermal management strategy is expected to provide both direct and indirect benefits. Weight reduction enhances vehicle dynamics and reduces material usage. Furthermore, in the context of Formula Student competitions, optimization studies are highly valuable as they contribute to increased points in static events, particularly in engineering design event. Improved overall vehicle performance may also lead to better lap times and consequently higher scores in dynamic events.

## Chapter 2

# Thermal Model

In this chapter, the thermal model developed to simulate the cooling system is introduced. This model is implemented in Simulink and utilizes Simscape physical blocks and signals. It is based on the cooling system architecture of the Oxford University Racing single-seater car for the 2023 season. As introduced in chapter 1, the system architecture features two independent and symmetrical systems on the right and left sides of the vehicle. For convenience, only one side will be considered throughout the discussion.

The team currently employs a powertrain design based on a 112V battery pack, two Plettenburg Nova-15 permanent magnet synchronous motors (PMSMs) [3] mounted on the rear axle, and an MST140-200 motor controller for each motor, manufactured by Plettenburg [4].

### 2.1 Cooling Loop

The architecture of the model follows the design choices made by the OUR team. The cooling system used during the 2023 season was designed to cool only the electric motor, while the inverter was air-cooled. Since the adoption of a cold plate

for inverter cooling is planned for future seasons, the cooling of the power modules will be introduced into the model. Consequently, the cooling of the inverter will be implemented using the model of the cold plate proposed by Dimitar Ruzhev in his desertation [5].

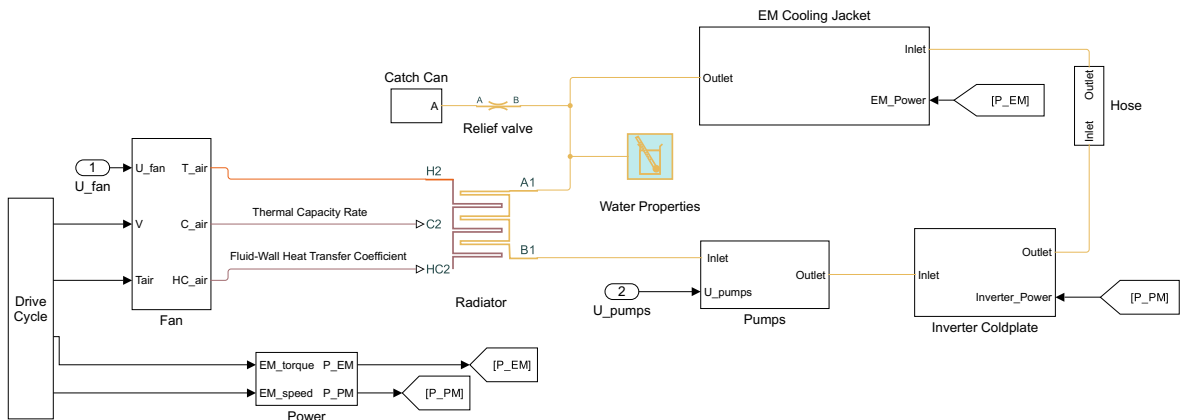


Figure 2.1: Model overview

Following the cooling loop, two EPB 15 Davies Craig pumps [1] are placed in series at the radiator outlet. Downstream of the pumps, the coldplate is positioned to cool the power modules. The cooling jacket for the electric motor is connected to the coldplate outlet. At the motor outlet, which is hypothetically the hottest point, the fluid returns to the radiator.

This configuration, referred to as the *Series Configuration*, serves as the baseline and will be used for all simulations and optimization studies. In ??, an alternative cooling loop will be tested, where the EM cooling jacket and the inverter cold plate are connected in parallel instead of in series. It will be observed that this latter configuration proves to be less advantageous.

## 2.2 Driving Cycle

During the 2022-23 season, the Oxford University Racing team conducted a test of the car.



Figure 2.2: Vehicle setup before the test

The vehicle data are reported below. The vehicle speed was measured using an IMU sensor.

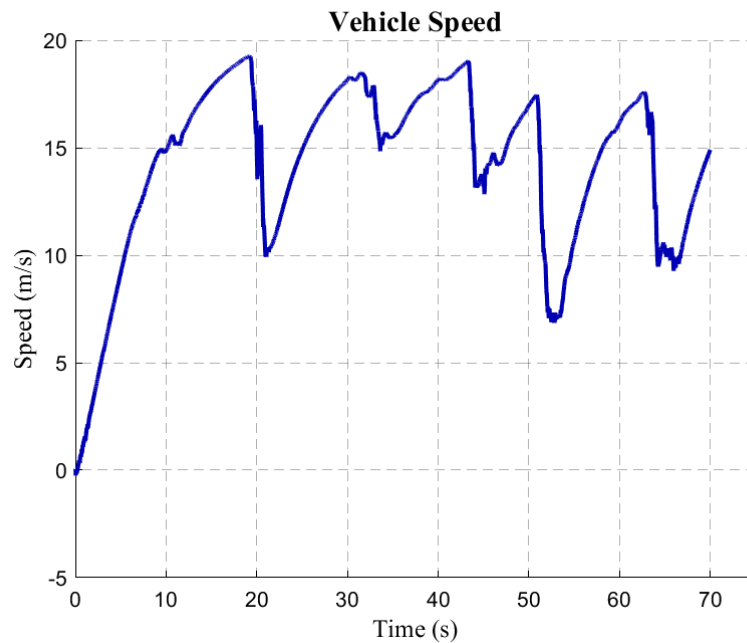


Figure 2.3: Vehicle speed plot

The vehicle speed plot (Figure 2.3) represents the reference cycle that was repeated to construct the cycle used in the simulations. The test was performed over a time interval of 70 seconds. The repetition of this cycle will constitute the reference cycle for the simulations.

Using a reluctance sensor and a hall effect sensor, data concerning motor speed and torque were collected.

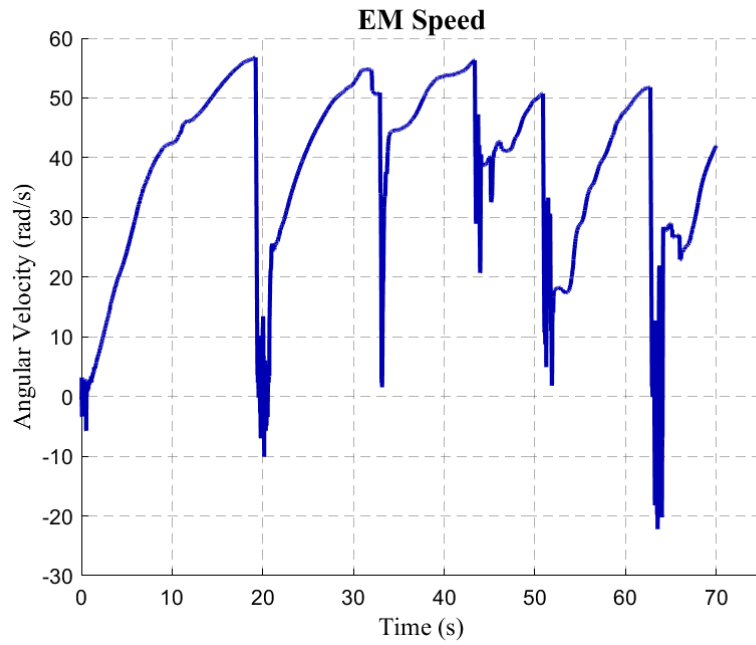


Figure 2.4: EM speed plot

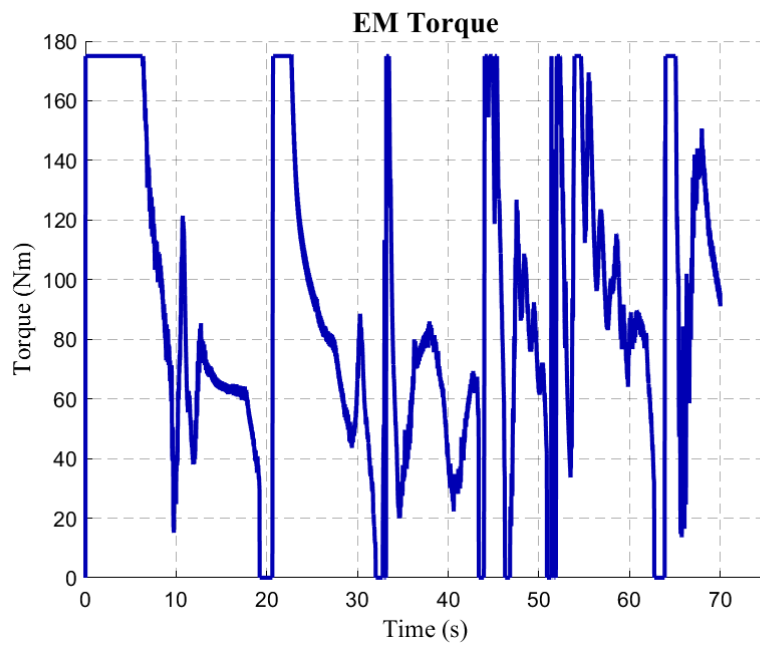


Figure 2.5: EM torque plot

A driving cycle block is used to build the simulation cycle. The reference driving cycle is repeated nine times. The total duration of the cycle used for the simulation is 630 seconds.

Through the MATLAB file `Loading_data.m`, it is possible to load a dataset containing driving cycle data. The dataset consists of multiple variables, including vehicle speed, electric motor speed, and electric motor torque. The dataset is loaded into the workspace, and the key variables are extracted.

```
Veh_Spd = repmat(data{1}.Values.Data, 9, 1);
EM_Spd = repmat(data{4}.Values.Data, 9, 1);
EM_Trq = repmat(data{6}.Values.Data, 9, 1);
```

These variables are essential for the subsequent simulations, as they represent the input driving conditions of the vehicle.

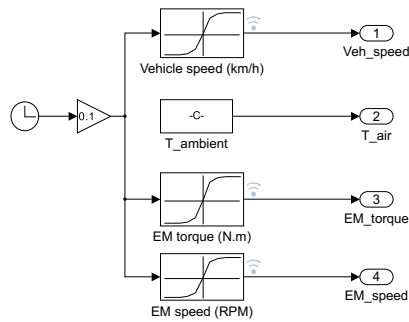


Figure 2.6: Driving cycle block

In the driving cycle block, the data are interpolated using a 1D lookup table,

considering a step time of 0.1 seconds. This block also retrieves the reference ambient temperature value from the workspace.

## 2.3 Electric Motor and Inverter Power Evaluation

The aim of this section is to properly evaluate the instantaneous power of the electric motor and the power required by the inverter's power modules.

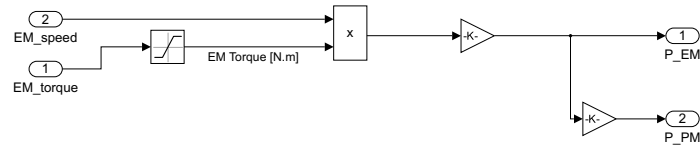


Figure 2.7: EM power block overview

$$P = T \cdot \omega \quad (2.1)$$

From the rotational dynamics equation (see Equation 2.1), the mechanical power value is obtained. The motor torque is saturated at a maximum value, which has been provided by the electric motor supplier[3].

It is possible to use the efficiency definition to compute the actual electrical power absorbed by the motor:

$$\eta_{EM} = \frac{P_{mech}}{P_{elec}} \quad (2.2)$$

From which we obtain:

$$P_{elec} = \frac{P_{mech}}{\eta_{EM}} \quad (2.3)$$

This value is then related to the inverter efficiency in order to compute the electrical power required by the inverter, using the following equation:

$$P_{inv} = \frac{P_{elec, EM}}{\eta_{inv}} \quad (2.4)$$

The output of this block is therefore the electrical power absorbed by both the electric motor and the inverter.

The mechanical efficiency of the electric machine is set to 85% [3]. The efficiency of the inverter is set to 96% [4].

## 2.4 Fan

This block models the cooling system fan. The fan is positioned downstream of the radiator, meaning its operating principle is based on the aspiration of air flowing through the radiator. The fan chosen are **San Ace 140 9GV 1412P1G001**.



Figure 2.8: San Ace 140 DC fan

Below is the datasheet of the fan.

Specification	Value
Manufacturer	San Ace
Product Category	DC Fan
Type	Axial Fan
Height	140 mm
Width	140 mm
Depth	38 mm
Operating Voltage	12 VDC
Airflow	310 CFM (9.5 m <sup>3</sup> /min)
Speed	7600 RPM
Bearing Type	Ball Bearing
Noise Level	70 dBA
IP Rating	IP20
Rated Power	55.2 W
Features	Speed Signal, Open Collector Output
Housing Material	Aluminum
Termination Style	Wire Leads - 4
Series	9GV
Current Type	DC

Table 2.1: Datasheet for San Ace 140 9GV1412P1G001 DC Axial Fan

The following Simulink block implements several relationships, specifically considering the fan's fluid dynamics, the thermodynamic variables related to heat exchange, and the control logic of the device.

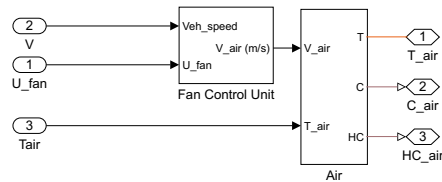


Figure 2.9: Fan block overview

### 2.4.1 Fan Control Unit

This subsystem defines the relation between the fan control variable and the air velocity interacting with the radiator fins. The control variable is associated to the PWM duty cycle.

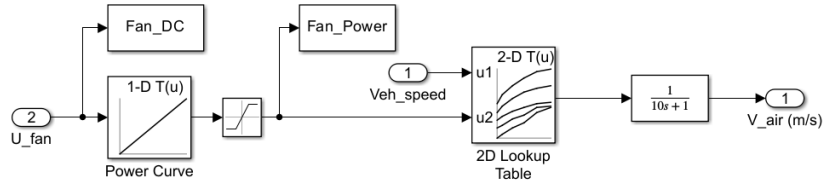


Figure 2.10: Fan control logic

Pulse Width Modulation (PWM) is a widely used technique for controlling the speed of electric fans by modulating the power supplied to the motor. Rather than adjusting the voltage continuously, PWM operates by rapidly switching the power supply on and off at a fixed frequency. The key parameter in this process is the duty cycle, which represents the proportion of time the signal remains in the "on" state within a complete cycle. A higher duty cycle results in increased fan speed, while a lower duty cycle reduces it accordingly.

The application of PWM in fan control varies depending on the type of fan. In this case the fan is equipped with four-wire that incorporate a dedicated PWM control input, allowing direct speed adjustment without interrupting the power supply. This method provides greater efficiency and precision in speed regulation.

The exit velocity of the fan is related to the vehicle's speed through a lookup table. This approach ensures that the airflow velocity through the radiator is accurately adjusted to the fluid dynamics, which depend on external conditions and the radiator's placement within the sidepod.

A low-pass filter is implemented to process the airflow output from a radiator fan, reducing high-frequency variations while preserving slower changes. This approach smooths the airflow signal by minimizing rapid fluctuations caused by turbulence, mechanical disturbances, or sudden variations in fan speed.

In a cooling system, airflow does not instantly affect temperature due to the thermal inertia of the radiator and coolant. A low-pass filter helps account for this delay, making the response more realistic. Additionally, airflow measurements often contain high-frequency noise from fan vibrations, turbulence, or sensor artifacts. Filtering these disturbances provides a cleaner signal, improving the accuracy of simulations and analyses.

In control applications, excessive sensitivity to rapid fluctuations can lead to instability or overly reactive adjustments. By smoothing the signal, the system responds more predictably, enhancing overall efficiency. The use of a low-pass filter thus ensures that airflow data better represents real cooling dynamics, making it more useful for modeling, regulation, and optimization

From the literature [6], 2.5 is chosen as transfer function.

$$H(s) = \frac{1}{10s + 1} \tag{2.5}$$

### 2.4.2 Thermodynamic Variables

This block computes the thermodynamic variables of air related to heat exchange in the air. Specifically, the heat capacity rate  $C$  and the heat transfer coefficient  $HC$  are evaluated.

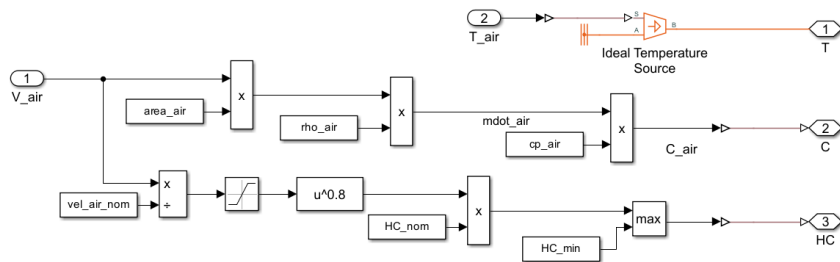


Figure 2.11: Air thermodynamic variables block

To compute the heat capacity rate  $C$ , we use the following equation:

$$\dot{m}_{\text{air}} = V_{\text{air}} \cdot A_{\text{fan}} \cdot \rho_{\text{air}} \quad (2.6)$$

$$C_{\text{air}} = \dot{m}_{\text{air}} \cdot c_{p,\text{air}} \quad (2.7)$$

The heat transfer coefficient  $HC$  is calculated as a function of the ratio between the actual air velocity and the nominal air velocity.

$$R = \frac{V_{\text{air}}}{V_{\text{air,nom}}} \quad (2.8)$$

$$HC = \max(HC_{\text{min}}, HC_{\text{nom}} \cdot R^{0.8}) \quad (2.9)$$

The term  $R^{0.8}$  indicates that the heat transfer increases with air velocity but at a diminishing rate (less than linear). The coefficient is also bounded by a minimum value ( $HC_{\text{min}}$ ) to prevent it from becoming too low under low airflow conditions.

The output of this subsystem consists of the values  $C$ ,  $HC$ , and the air temperature converted into a Simscape signal.

## 2.5 Radiator

This SimScape block models a heat exchanger in a thermal liquid network. Heat is transferred to an external fluid whose flow is controlled by physical signal inputs. The block is set up based on the **Epsilon-NTU method** for heat exchangers. The Epsilon-NTU method is commonly used to model heat exchangers, especially when the temperature and flow rate are not constant. The method is based on the concept of heat exchanger effectiveness ( $\epsilon$ ) and the number of transfer units

(NTU). It is used to estimate the heat transfer rate in systems with complex configurations. The general relationship is given by:

$$Q = \epsilon \cdot C_{\min} \cdot (T_{\text{hot, in}} - T_{\text{cold, in}})$$

Where:

- $Q$  is the rate of heat transfer.
- $\epsilon$  is the effectiveness of the heat exchanger.
- $C_{\min}$  is the minimum heat capacity rate.
- $T_{\text{hot, in}}$  and  $T_{\text{cold, in}}$  are the inlet temperatures of the hot and cold fluids, respectively.

The geometry of the internal channels of the radiator is modeled as a cross-flow heat exchanger. In this configuration, the two fluids (the air and the thermal liquid) flow perpendicular to each other. In automotive applications, this configuration is typical for radiators where the cooling liquid flows through the tubes while air flows across the tubes, providing an efficient mechanism for heat exchange.

The wall thermal resistance is calculated as:

$$R_{\text{wall}} = \frac{0.014}{381 \cdot n_{\text{tubes}} \cdot w_{\text{radiator}} \cdot L_{\text{tube}}}$$

Where:

- 0.014 is a constant related to the thermal conductivity of the tube material.
- 381 is a constant factor that accounts for the efficiency of heat transfer in the tubes.
- $n_{\text{tubes}}$  is the number of tubes in the radiator.

- $w_{\text{radiator}}$  is the width of the radiator.
- $L_{\text{tube}}$  is the length of the tubes.

This equation is derived from standard engineering practices for modeling heat transfer in heat exchangers.

The minimum free flow area is defined as:

$$A_{\text{min}} = n_{\text{tubes}} \cdot (w_{\text{radiator}} \cdot h_{\text{tube}})$$

Where:

- $n_{\text{tubes}}$  is the number of tubes.
- $w_{\text{radiator}}$  is the width of the radiator.
- $h_{\text{tube}}$  is the height of the tubes.

This value represents the total cross-sectional area available for the fluid flow through the radiator.

The hydraulic diameter for pressure loss is defined as:

$$D_h = \frac{4 \cdot (w_{\text{radiator}} \cdot h_{\text{tube}})}{2 \cdot (w_{\text{radiator}} + h_{\text{tube}})}$$

Where:

- $w_{\text{radiator}}$  is the width of the radiator.
- $h_{\text{tube}}$  is the height of the tubes.

This equation provides the characteristic diameter used to evaluate pressure losses due to fluid flow within the tubes.

The thermal liquid volume is defined as the total volume of the thermal liquid that passes through the radiator, calculated as:

$$V_{\text{thermal liquid}} = n_{\text{tubes}} \cdot (w_{\text{radiator}} \cdot h_{\text{tube}}) \cdot L_{\text{tube}}$$

Where:

- $n_{\text{tubes}}$  is the number of tubes.
- $w_{\text{radiator}}$  is the width of the radiator.
- $h_{\text{tube}}$  is the height of the tubes.
- $L_{\text{tube}}$  is the length of the tubes.

This volume represents the total amount of liquid in the radiator that interacts with the heat exchange process.

The upper Reynolds number limit for laminar flow is set to 2000 and the upper Reynolds number limit for turbulent flow is set to 4000. These values are used to distinguish between laminar and turbulent flow regimes in the radiator tubes.

The roughness of the internal channels is chosen as  $15 \times 10^{-6}$ , based on [7]. This roughness value is crucial for calculating the friction losses in the radiator tubes.

The heat transfer surface area for the thermal liquid is defined as:

$$A_{\text{thermal liquid}} = n_{\text{tubes}} \cdot 2 \cdot (L_{\text{tube}} \cdot w_{\text{radiator}} + L_{\text{tube}} \cdot h_{\text{tube}})$$

Where:

- $n_{\text{tubes}}$  is the number of tubes.
- $L_{\text{tube}}$ ,  $w_{\text{radiator}}$ , and  $h_{\text{tube}}$  are the dimensions of the radiator tubes.

For the air, the heat transfer surface area is defined as:

$$A_{\text{air}} = A_{\text{primary}} + A_{\text{fins}}$$

Where:

- $A_{\text{primary}}$  is the surface area of the primary section of the radiator.
- $A_{\text{fins}}$  is the surface area of the fins that enhance heat transfer.

The initial temperature of the cooling liquid is defined as 293.15 K, which is equivalent to  $293.15 - 273.15 = 20^\circ\text{C}$ .

The initial pressure is set at 0.101325 MPa, which is equivalent to:

$$P_{\text{initial}} = 0.101325 \text{ MPa} = 1 \text{ atm}$$

## 2.6 Pumps

This block models the pumps used in the cooling system. The reference pump is the **Davies Craig EBP15** [1].



Figure 2.12: Davies Craig EBP15 DC pump

In the cooling system proposed by OUR for the 2023 season, two pumps are arranged in series. This configuration has been implemented as a safety measure to ensure that, in case of a failure, the liquid continues to circulate. This choice

was also influenced by the lack of in-depth knowledge regarding pressure losses along the circuit.

<b>Specification</b>	<b>Value</b>
<b>Max Flowrate</b>	22.7 L/min
<b>Rated Flowrate</b>	15 L/min (4 US gal/min) @ 10 kPa
<b>Motor Type</b>	12 Volt Brushless
<b>Operating Voltage</b>	9V DC to 15V DC
<b>Maximum Current</b>	1.3 A
<b>Max Pump Pressure</b>	0.2 Bar (2.9 psi)
<b>Operating Temperature</b>	-40°C to 120°C (-40°F to 248°F)
<b>Pump Design</b>	Recirculating Centrifugal
<b>Pump Weight</b>	245 grams (0.54 lb)
<b>Pump Material</b>	Nylon 66, 30% glass-filled
<b>Self Priming</b>	No, not self-priming
<b>Burst Pressure</b>	250 kPa (36 psi) minimum
<b>Fits Hose Sizes</b>	12.5mm to 19mm (½" to ¾")
<b>Max Head Height</b>	2.4 m
<b>Rated Voltage</b>	12V

Table 2.2: Datasheet for Davies Craig EBP15 Electric Booster Pump

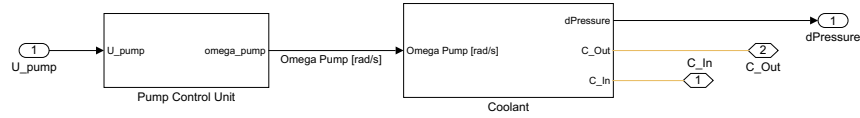


Figure 2.13: Pumps block

To consider the effect of the pump in the model, Centrifugal Pump block is used. This block models a centrifugal pump in a thermal liquid network. The reference pump characterization is based on head and brake power as a function of pump capacity.

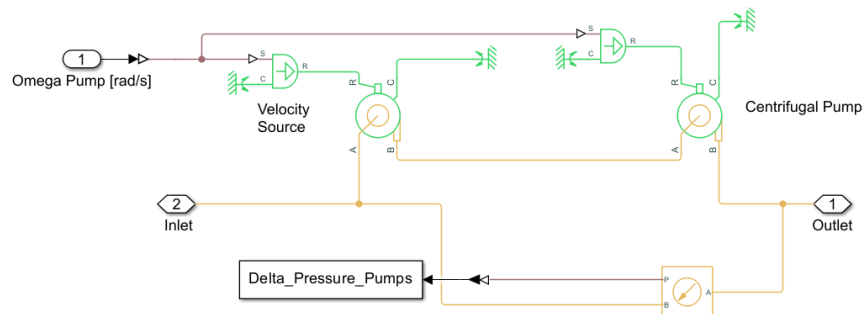


Figure 2.14: Pumps coolant fluid dynamics modeling

The heat exchange in the cooling system is governed by the thermal power equation:

$$Q = \dot{m}c_p\Delta T \quad (2.10)$$

where:

- $Q$  is the heat power exchanged [W],
- $\dot{m}$  is the mass flow rate [kg/s],
- $c_p$  is the specific heat capacity of the coolant [J/kgK],
- $\Delta T$  is the temperature difference between the inlet and outlet of the heat exchanger [K].

The mass flow rate is related to the volumetric flow rate by:

$$\dot{m} = \rho Q_v \quad (2.11)$$

where:

- $\rho$  is the density of the coolant [kg/m<sup>3</sup>],
- $Q_v$  is the volumetric flow rate [m<sup>3</sup>/s].

The velocity of the fluid can be related to the volumetric flow rate as:

$$v = \frac{Q_v}{A} \quad (2.12)$$

where  $A$  is the cross-sectional area of the pipe [m<sup>2</sup>].

Since the pumps are in series, the flow rate remains unchanged, while the pressure drop imposed in the cooling system increases. This results in a lower risk of cavitation, as cavitation occurs when the local pressure drops below the vapor pressure of the fluid:

$$P_{extlocal} < P_{extvapor} \quad (2.13)$$

By increasing the overall system pressure, cavitation is less likely to occur.

A pressure sensor is also integrated into the model to monitor system performance and ensure optimal operation.

### 2.6.1 Pumps Control Unit

In the Simulink model, the control variable for the centrifugal pump block is the imposed shaft speed. For the purpose of this thesis, a new control variable,  $U_{\text{pump}}$ , will be defined to represent the PWM duty cycle. This variable will be related to the actual value of power and then through a lookup table to the rotational speed of the pump shaft, establishing a correlation between  $U_{\text{pump}}$  and the angular velocity of the pump impeller.

A gain is introduced to account for the transmission ratio between the shaft and the rotor. Since the shaft is rigidly connected to the rotor, this gain is set to unity, ensuring a direct relationship between the imposed shaft speed and the rotor's angular velocity.

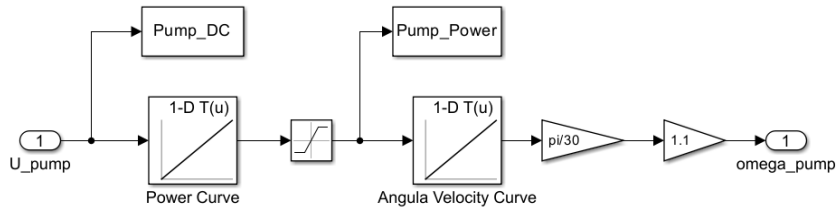


Figure 2.15: Pumps control unit

## 2.7 Inverter Cold Plate

In this section, the inverter cold plate is modeled. The input of the block is the electric power requested by the inverter, evaluated in Section 2.3. This data is

associated with a gain that accounts for the amount of power dissipated as heat.

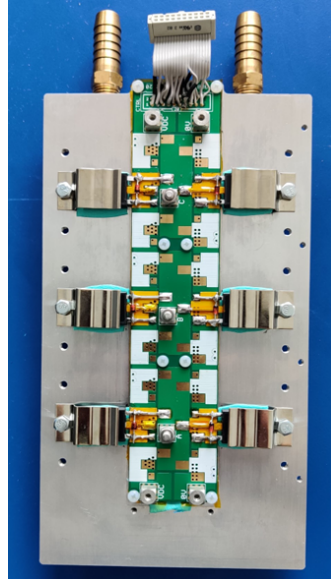


Figure 2.16: Inverter cold plate

In inverters, power losses primarily arise from:

- Switching losses: Due to the finite switching time of semiconductor devices.
- Conduction losses: Resulting from the internal resistance of power components.
- Thermal losses: Generated by the heat dissipated in semiconductors and other components.
- Parasitic losses: Caused by leakage currents and electromagnetic effects.

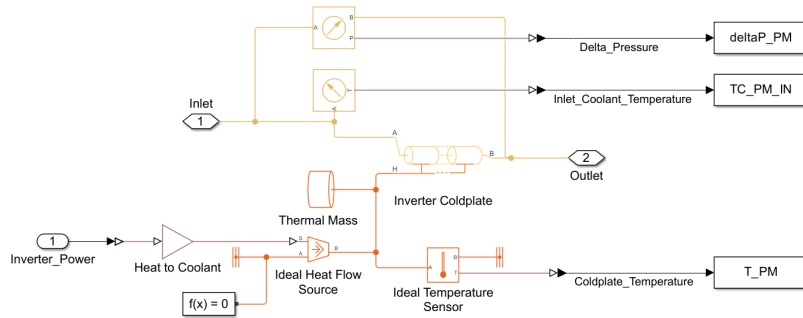


Figure 2.17: Inverter block

According to the literature [8] and the studies conducted during the theses cited here [9] [5], a value of 3.7% represents a realistic percentage of the inverter’s electrical power that is dissipated as heat.

Using Simscape, the Ideal Heat Flow Source block is employed to convert the thermal power into a Simscape physical signal (orange signal).

To account for the contribution of the coldplate mass in heat exchange, the Coolant Loop Thermal Mass block is used. This block models internal energy storage in a thermal network. The rate of temperature increase is proportional to the heat flow rate into the material and inversely proportional to the mass and specific heat of the material.

To simulate the cold plate walls, a Simscape Pipe block is utilized. This block models pipe flow dynamics in a thermal liquid network, considering viscous friction losses and convective heat transfer with the pipe wall. The effects of dynamic compressibility, fluid inertia, elevation, and wall compliance can be optionally included.

Geometric data of the cold plate is incorporated within the model. We refer to the cold plate proposed for the motor controller by Dimitri Ruzhev [5].

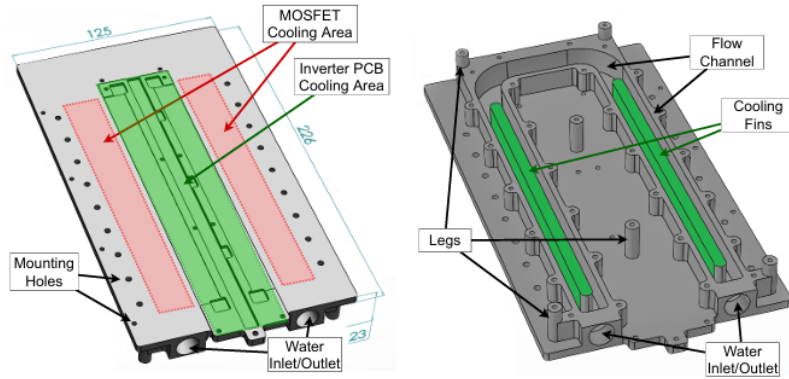


Figure 2.18: Inverter cold plate internal view

The internal duct geometry is circular, with a total of three segments. The geometric data and the associated pressure losses of the cold plate are inserted into the model.

Heat transfer parameterization is performed using tabulated data, specifically Nusselt number vs. Reynolds number vs. Prandtl number.

The initial pressure is defined as:

$$P_0 = 0.101325 \text{ MPa} \quad (= 1 \text{ bar}) \quad (2.14)$$

The initial temperature is set to:

$$T_0 = 303.15 \text{ K} \quad (= 30^\circ\text{C}) \quad (2.15)$$

The output of the Pipe block is a physical signal containing information about the thermodynamic state of the coolant at the inlet.

Using appropriate sensors model, it is possible to measure the temperature at the inlet of the cold plate and the pressure drop imposed by the cold plate.

The outlet temperature is measured using an Ideal Temperature Sensor block.

## 2.8 Hose

To evaluate and account for the pressure drop imposed by the pipes, Pipe block is used. The fittings pressure drop within the cooling circuit are neglected. The geometric parameters present in this block were obtained through measurements performed on the cooling system at the OUR team laboratory. The parameters related to pipe losses were sourced from the literature [10].

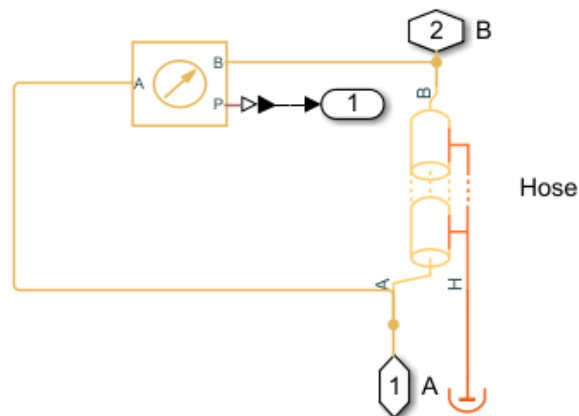


Figure 2.19: Hose block

Considering the material, which in this case is rubber, the appropriate parameters are selected accordingly.

For simplicity, the pipes are assumed to be perfectly insulated. This assumption is acceptable for the purposes of our research. A pressure sensor is used to monitor the pressure drop imposed by the pipes in the circuit.

## 2.9 Electric Motor Cooling Jacket

The electric motor is modeled in a Simulink subsystem. The cooling of the electric motor is achieved through a cooling jacket that wraps around the motor. Inside the cooling jacket, the coolant flows. The cooling jackets used are those provided by the motor supplier. Inside, there is a single channel which surrounds the motor case.



Figure 2.20: Plettenburg Nova-15 permanent magnet synchronous motors (PMSMs)

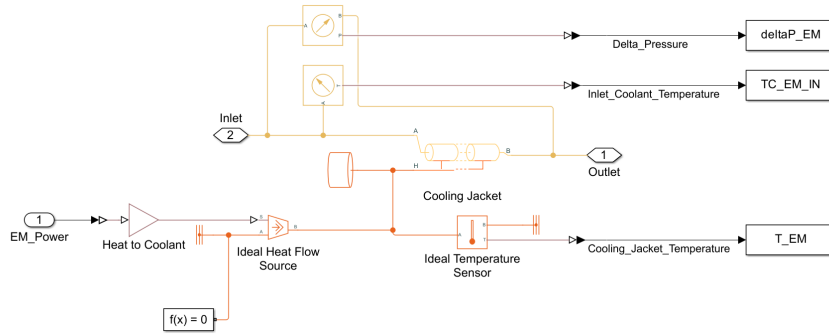


Figure 2.21: EM block overview

Starting from the input of the electric power of the motor, previously calculated in Section 2.3, this is related through a gain that defines the percentage of power dissipated as heat. A value of 12% is chosen based on the literature.[11]

This data is then converted into a physical Simulink signal. This signal is related to the mass involved in the heat exchange, referring to the mass of the motor plus the cooling jacket.

The geometric parameters used in the block were measured at the OUR team laboratory or obtained from the motor provider’s datasheet.[3]

To simulate the cooling jacket walls, a Simscape Pipe block is utilized. This block models pipe flow dynamics in a thermal liquid network, considering viscous friction losses and convective heat transfer with the pipe wall. The effects of dynamic compressibility, fluid inertia, elevation, and wall compliance can be optionally included.

The internal duct geometry is approximated with a single segment. The pressure losses associated to the cooling jacket are obtained from its datasheet.

Heat transfer parameterization is performed using tabulated data, specifically Nusselt number vs. Reynolds number vs. Prandtl number.

The initial pressure is defined as:

$$P_0 = 0.101325 \text{ MPa} \quad (= 1 \text{ atm}) \quad (2.16)$$

The initial temperature is set to:

$$T_0 = 303.15 \text{ K} \quad (= 30^\circ\text{C}) \quad (2.17)$$

The output of the Pipe block is a physical signal containing information about the thermodynamic state of the coolant at the inlet.

Using appropriate sensors, it is possible to measure the temperature at the inlet of the cooling jacket and the pressure drop imposed by the channel.

The outlet temperature is measured using an Ideal Temperature Sensor block.

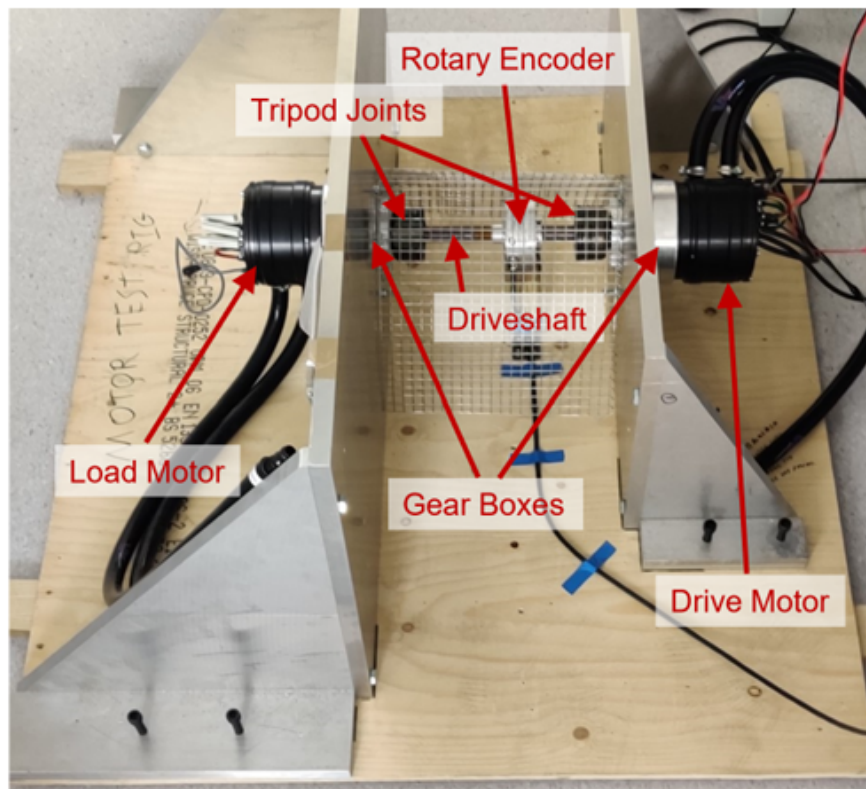


Figure 2.22: EM test rig

## 2.10 Catch Can

The presence of a catch can is a fundamental requirement dictated by the regulations of Formula Student competitions.[12] Its role is to ensure the possibility of fluid expansion without causing complications in terms of safety and the correct operation of the cooling system.

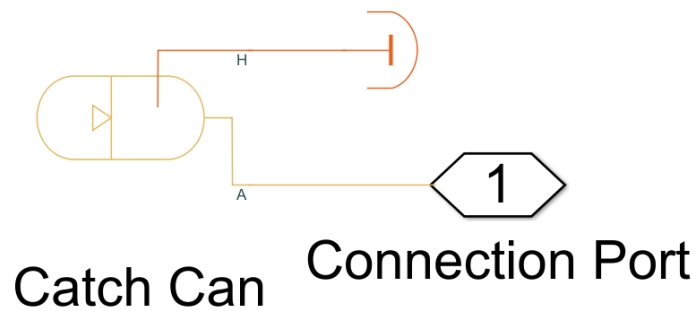


Figure 2.23: Catch can model

In Simulink, this component is simulated using a block that models a gas-charged thermal liquid accumulator. The accumulator consists of a precharged gas chamber and a liquid chamber. The liquid chamber is connected to a thermal liquid network.

The volume is defined as:

$$V = 1.5 \text{ dm}^3 = 1.5L \quad (2.18)$$

The initial pressure is set to zero.

At the inlet of the catch can, a relief valve is positioned. This block models the pressure loss due to a flow area restriction in a thermal liquid network. The ratio is set as fixed. The restriction area is:

$$A_r = \pi \times (0.001)^2 \text{ m}^2 \quad (2.19)$$

while the cross-sectional area of the inlet and outlet pipes is:

$$A_c = \pi \times (0.005)^2 \text{ m}^2 \quad (2.20)$$

# Chapter 3

## Simulations

### 3.1 Sensitivity Analysis

The purpose of this section is to run simulations to test the sensitivity of the model to variations in selected variables. This approach allows us to evaluate the dynamics of the model and determine its response to changes in specific parameters. By analyzing the trends, we can also gain insights into the robustness of the model.

Sensitivity analysis plays a crucial role in validating the accuracy and reliability of the developed model. It helps identify the most influential parameters and assess the impact of their variations on the system's overall performance. By systematically adjusting these parameters and observing the model's behavior, we can better understand its limitations and potential areas for improvement.

Additionally, performing multiple simulations provides a comprehensive overview of the model's stability under different operating conditions. If the model exhibits consistent behavior despite parameter variations, it suggests a high level of robustness. Conversely, significant deviations might indicate areas that require further refinement or additional constraints.

These simulations also serve as a preliminary step for optimization, enabling us to fine-tune the model for better accuracy and predictive capability. The results obtained from sensitivity analysis can be used to guide future development and improve the model's practical applicability.

### 3.1.1 Ambient Temperature Analysis

First, the effect of ambient temperature on the cooling system is analyzed. The ambient temperature ( $T_{\text{amb}}$ ) is varied between 20°C and 35°C, and the cooling system's response is observed.

```
T_Amb_Vector = {  
    20, 'g', '20 °C';  
    25, 'r', '25 °C';  
    30, 'b', '30 °C';  
    35, 'c', '35 °C'  
};
```

Each simulation corresponds to a different ambient temperature, and the temperature of the electric motor at the outlet is plotted. This analysis demonstrates how changes in external conditions, such as ambient temperature, can influence the cooling system's ability to dissipate heat.

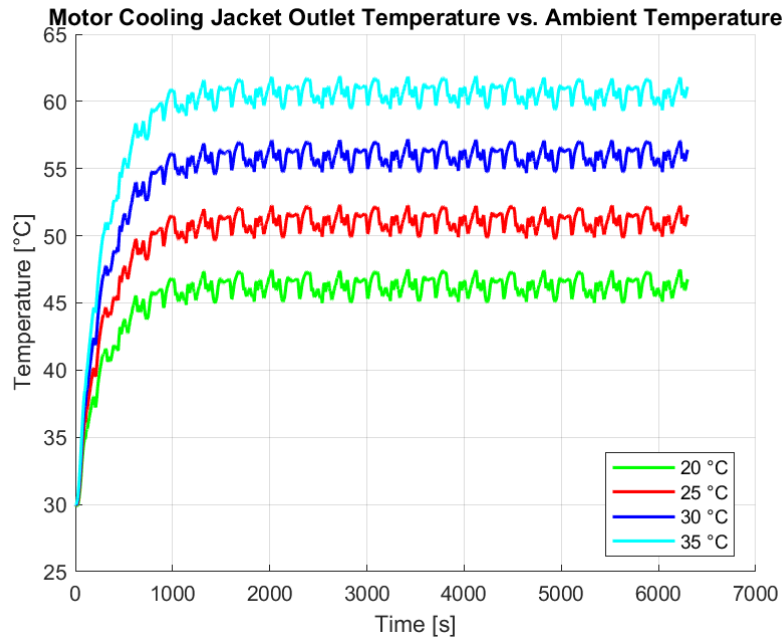


Figure 3.1: Variation of EM outlet temperature as a function of ambient temperature

### 3.1.2 Inverter Efficiency Settings Analysis

The cooling system is further analyzed under varying the efficiency of the inverter. A decrease in the efficiency result in a increase in the thermal losses, and consequently more thermal power required to be dissipated. The thermal losses of is represented as a gain, with values ranging from 5% to 15% of the full power.

```
Losses_PM_Vector = {
    0.05, 'g', '5%';
    0.07, 'r', '7%';
    0.10, 'b', '10%';
    0.15, 'c', '15%'
};
```

The system is simulated under each power setting, and the temperature at the

outlet of the power module is plotted. This analysis illustrates how the cooling system performs when the inverter operates in different efficiency conditions.

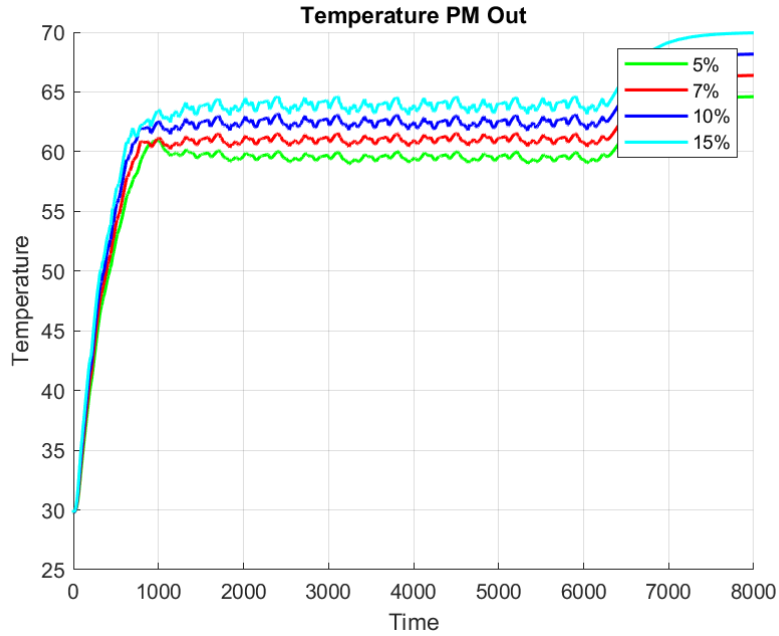


Figure 3.2: Variation of coldplate outlet temperature as a function of inverter efficiency

### 3.1.3 Fan Control Settings Analysis

The following analysis examines the behavior of the cooling system as the radiator fan control parameter is varied. Different operating conditions are evaluated, each corresponding to a different fan power level. As the fan power changes, the speed through the radiator varies, and consequently, the heat exchange between the cooling loop and the external environment is affected.

```

U_fan_Vector = {
    10, 'Fan Setting: 10%';
    25, 'Fan Setting: 25%';
    50, 'Fan Setting: 50%';
    75 , 'Fan Setting: 75%';
    100, 'Fan Setting: 100%'
};

```

The simulation results in temperature profiles for the electric motor, which are plotted for each fan setting.

Two plots are generated: 3.3 shows the temperature of the electric motor at the outlet.

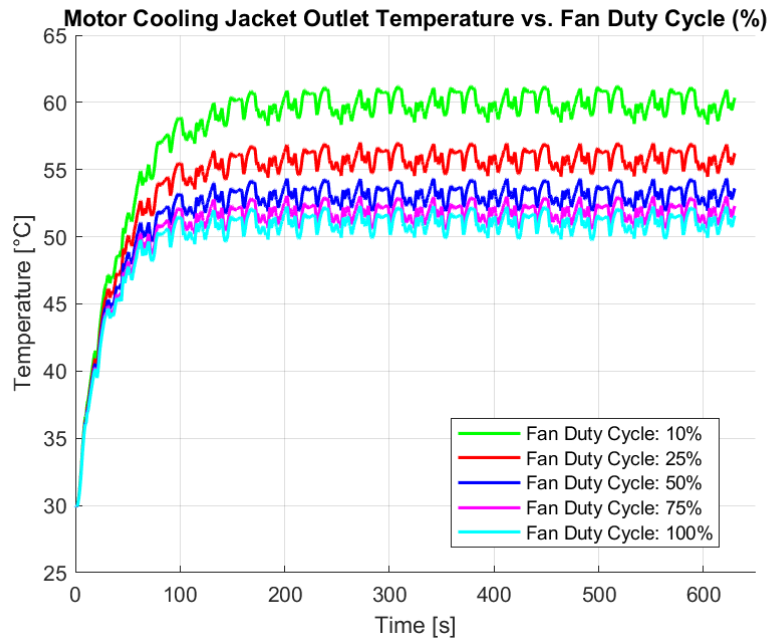


Figure 3.3: Variation of EM outlet temperature as a function of fan control settings

It is also worth it to highlight the difference of temperature between the inlet and the outlet changing the fan setting. The figure 3.4 shows the temperature

difference between the inlet and outlet of the electric motor ( $\Delta T$ ). This analysis provides insight into how varying fan settings affect the cooling performance.

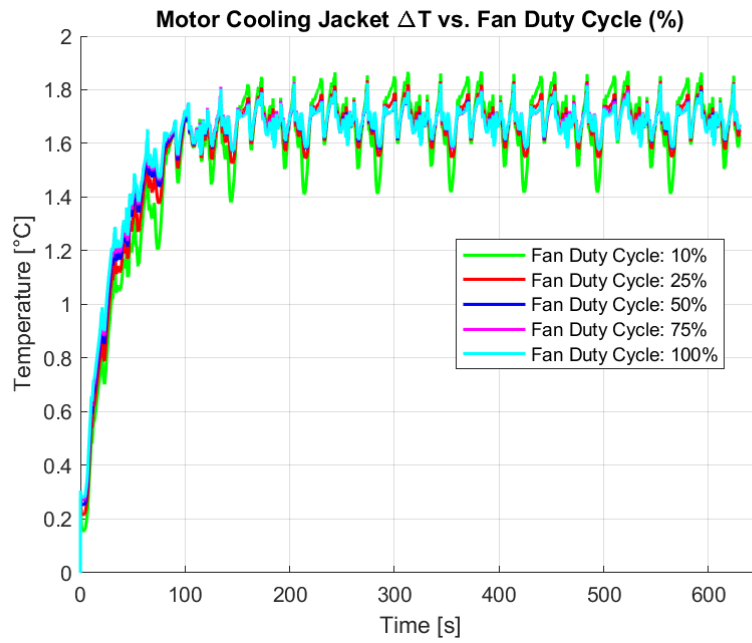


Figure 3.4: Variation of  $\Delta$  temperature across the EM cooling jacket as a function of fan control settings

Similarly, the following plots show the influence of fan control variation on the temperature recorded on the inverter and the temperature gradient achievable between the inlet and outlet of the cold plate.

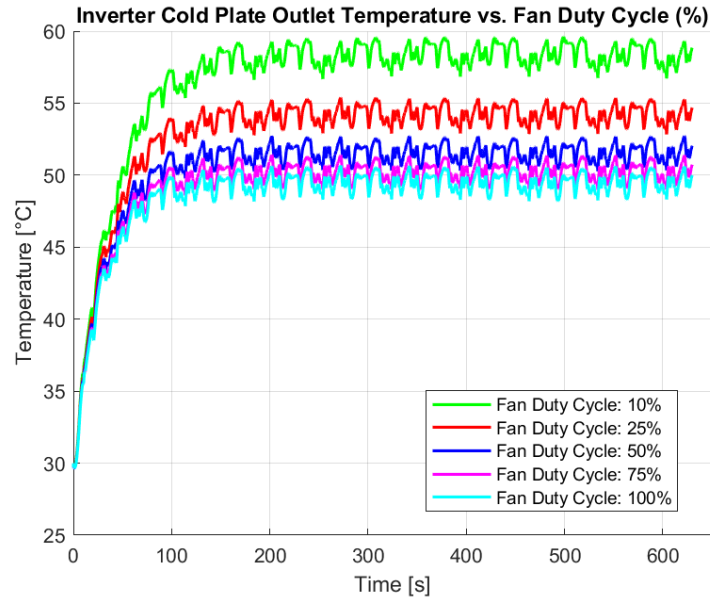


Figure 3.5: Variation of PM outlet temperature as a function of fan control settings

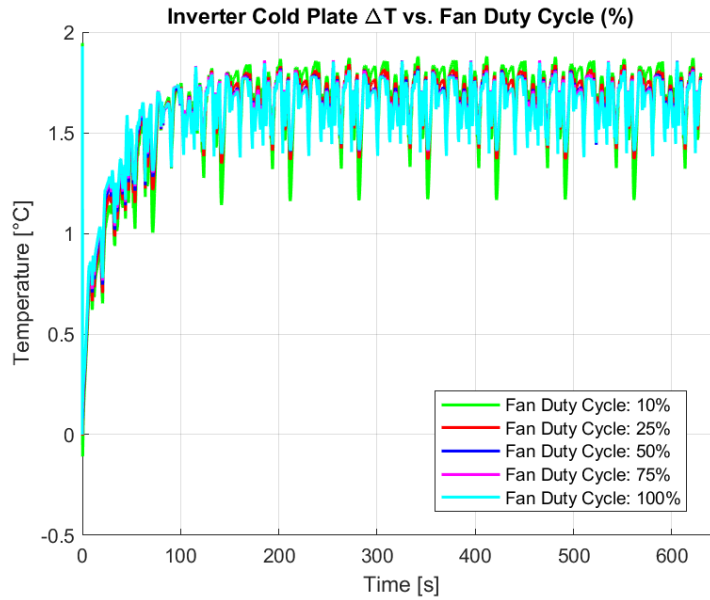


Figure 3.6: Variation of  $\Delta$  temperature across the PM cooling plate as a function of fan control settings

### 3.1.4 Pump Control Settings Analysis

Following the same workflow of 3.1.3, the behavior of the cooling system is analyzed changing the pump control variable.

```
U_pump_Vector = {  
    10, 'Pumps Setting: 10%';  
    25, 'Pumps Setting: 25%';  
    50, 'Pumps Setting: 50%';  
    75, 'Pumps Setting: 75%';  
    100, 'Pumps Setting: 100%'  
};
```

Each row in the matrix defines a control settings for the duty cycle.

The simulation results in temperature profiles for the electric motor, which are plotted for each pump setting.

The following section presents four plots illustrating the influence of pump settings on the temperatures recorded in the main components and the system's ability to dissipate heat. Particular attention is given to plot 3.9, which highlights the strong dependence of the electric motor temperature on pump variations. This will be useful in Chapter 4 for implementing a PID-based control strategy.

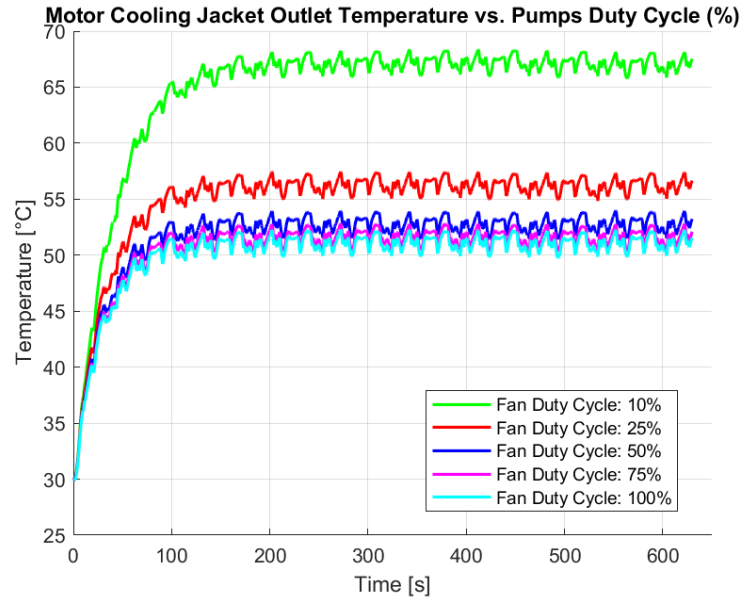


Figure 3.7: Variation of EM cooling jacket outlet temperature as a function of pumps control settings

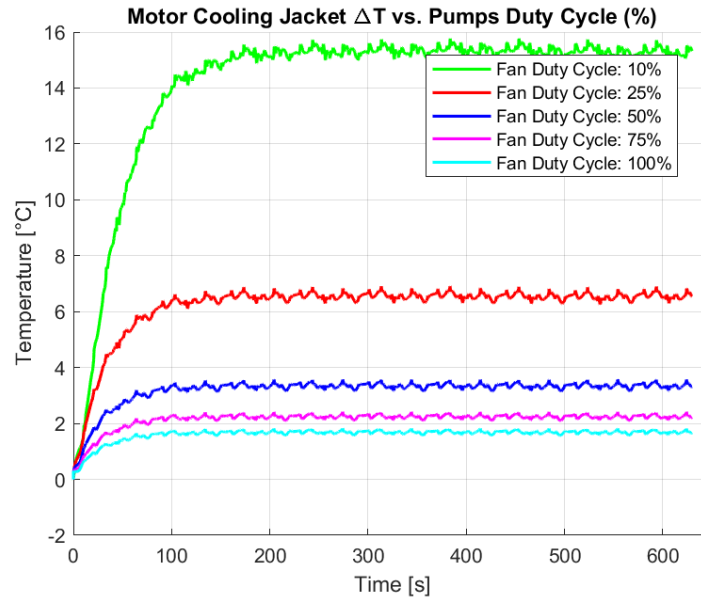


Figure 3.8: Variation of  $\Delta$  temperature across the EM cooling jacket as a function of pump control settings

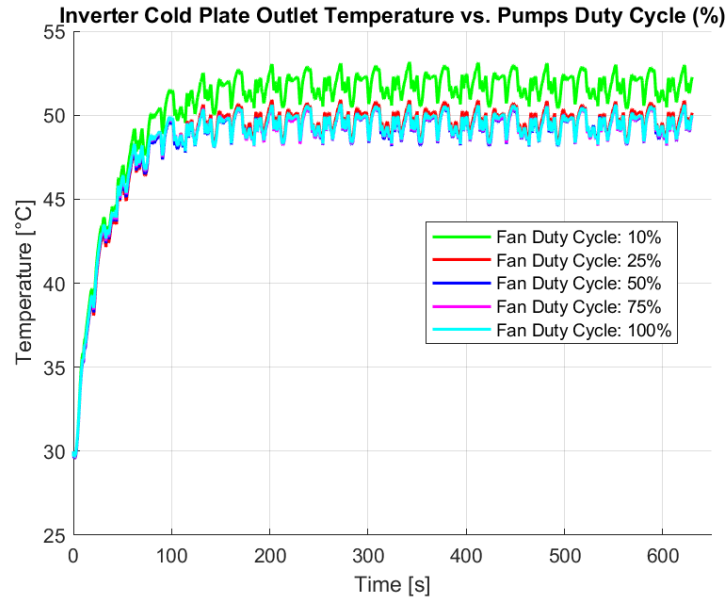


Figure 3.9: Variation of PM cold plate outlet temperature as a function of pumps control settings

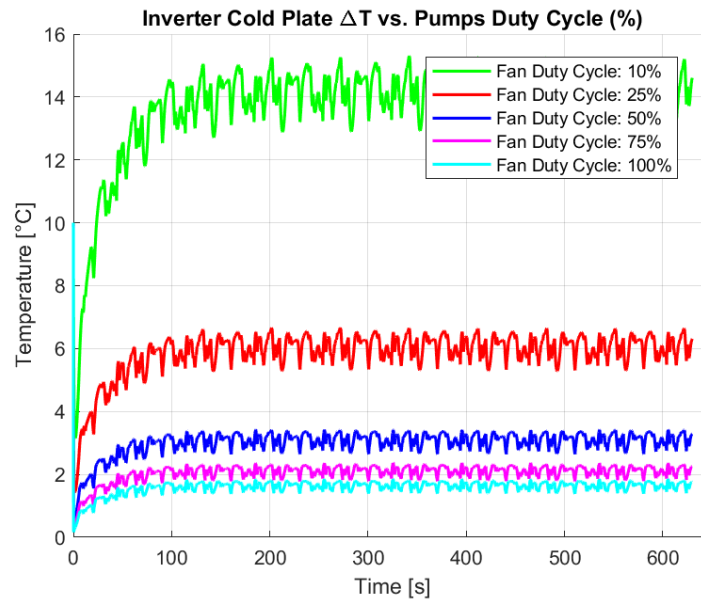


Figure 3.10: Variation of  $\Delta$  temperature across the PM cold plate as a function of pump control settings

## **3.2 Full Power Configuration**

This section analyzes the behavior of the cooling system under non-optimized conditions. In the absence of a thermal management strategy, the cooling system operates in a mode that ensures maximum heat dissipation. As a result, the fan settings are at full power, ensuring the highest air flow through the radiator. Similarly, the pump settings are also at full power, ensuring maximum flow rate within the cooling system. This configuration ensures a safe condition, as it provides the maximum temperature reduction for the powertrain components.

### **3.2.1 Temperature Analysis**

The following plots show the temperature signals for the electric motor and the inverter. These plots will serve as the baseline for the optimization process. As previously mentioned, a full power condition for the auxiliaries of the cooling system ensures the highest temperature reduction. By fully utilizing the potential of the cooling system, it is possible to dissipate the maximum amount of heat from the cooling loop.

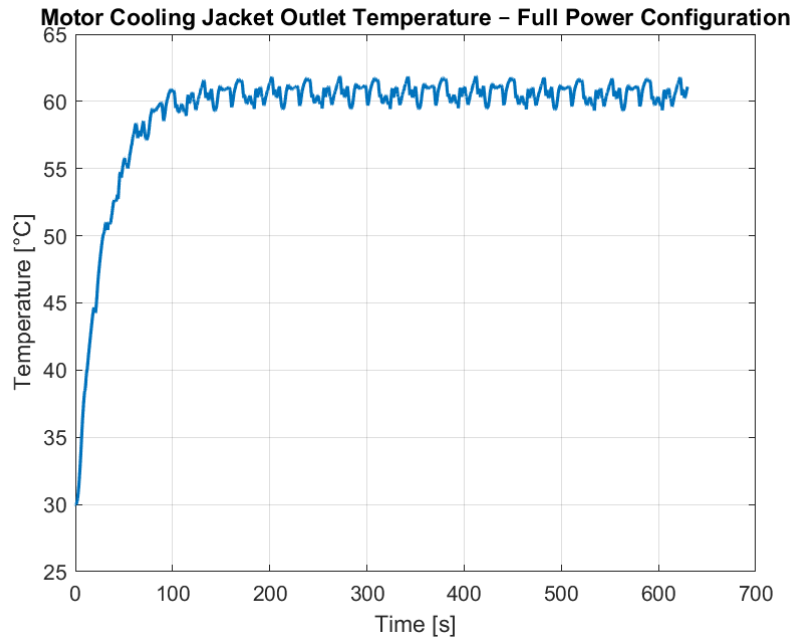


Figure 3.11: Motor cooling jacket outlet temperature in full power configuration

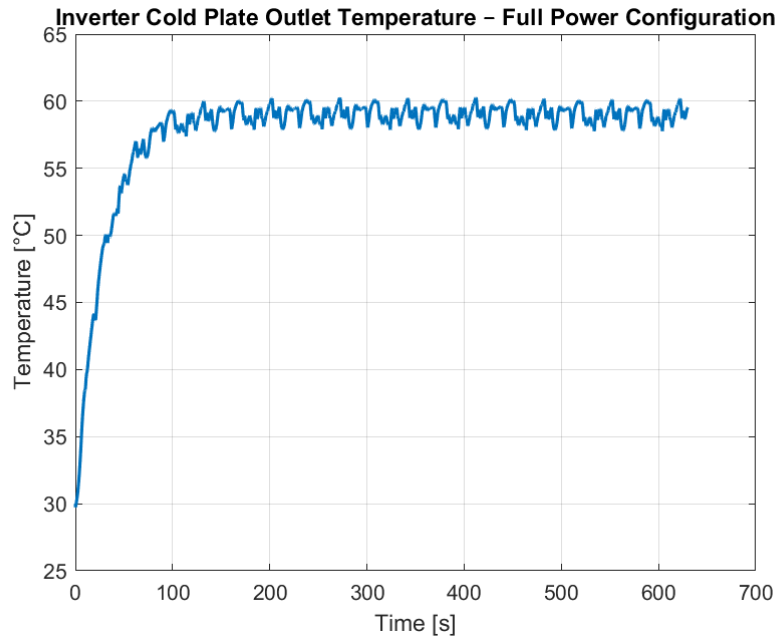


Figure 3.12: Inverter cold plate outlet temperature in full power configuration

### 3.2.2 Energy Consumption

In full power, the highest energy consumption is required by the auxiliary systems, namely the pumps and fans. The LV battery pack must therefore be sized to accommodate the maximum energy expenditure of the cooling system to prevent the auxiliaries from shutting down. Below, the energy consumption in this configuration will be examined in order to establish a baseline value to optimize in Chapter 4.

The energy consumed by the auxiliaries can be calculated using the following equation:

$$\text{Energy} = \int P dt \xrightarrow{\text{if } P \text{ is constant}} = P \cdot t \quad (3.1)$$

The control of the devices is performed via PWM (Pulse Width Modulation). This is a technique used to control the power delivered to electrical devices by varying the width of the pulses in a signal. It involves switching the signal on and off at a high frequency, and by adjusting the duration of the "on" time (duty cycle), it controls the average power supplied to the device. The duty cycle is therefore related to the actual power through a power curve.

The equation 3.1 is implemented in MATLAB and the cumulative energy consumption during the simulation is plotted. It is worth to underline that the trend is linear because the power is constant. From the fan datasheet [2], it is possible to observe that under full power condition, with 100% PWM duty cycle, the following parameters can be measured.

$$\text{Rated Current} = 4.6\text{A}$$

$$\text{Rated Power} = 55.2\text{W}$$

Considering the simulation time of 620 seconds and considering a full power utilization we can evaluate the energy consumption.

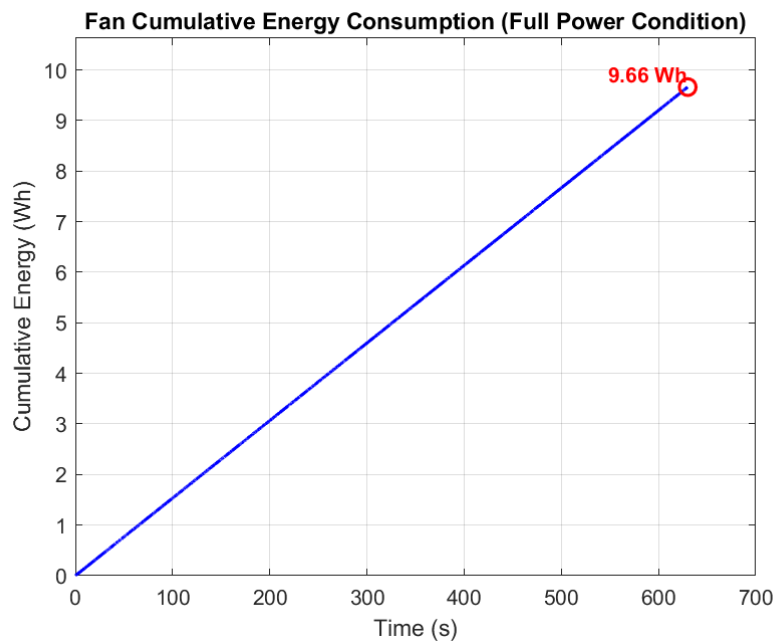


Figure 3.13: Fan energy consumption in full power configuration

Analyzing the pump datasheet [1], it is possible to observe that under full power condition, with 100% PWM, the following parameters can be measured.

Rated Current = 1.9A

Rated Power = 23.6W

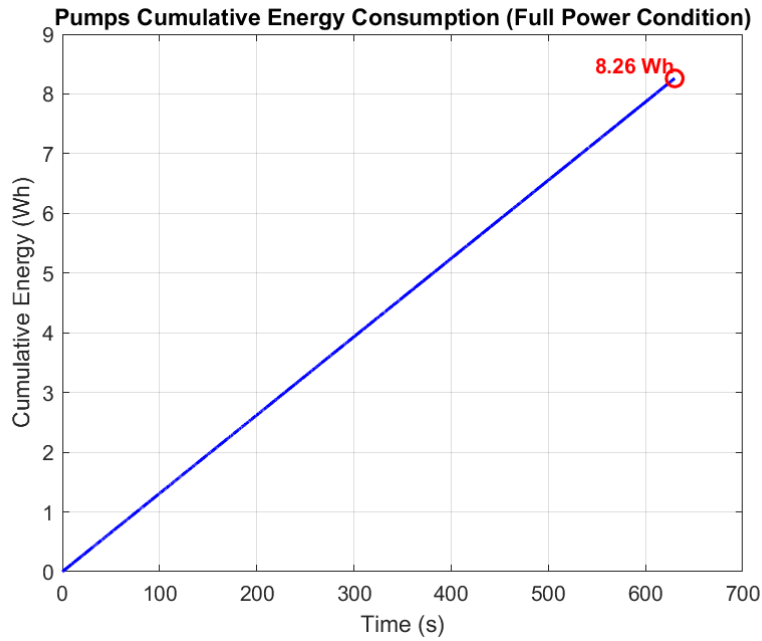


Figure 3.14: Pump energy consumption in full power configuration

It has already been stated that the circuit includes two pumps; therefore, 3.14 represents the total consumption of both users.

Considering both the contribution of the auxiliary systems and assuming that the contribution of the other cooling system devices is negligible, the energy required by one side of the cooling system to the LV battery pack is plotted in the following graph.

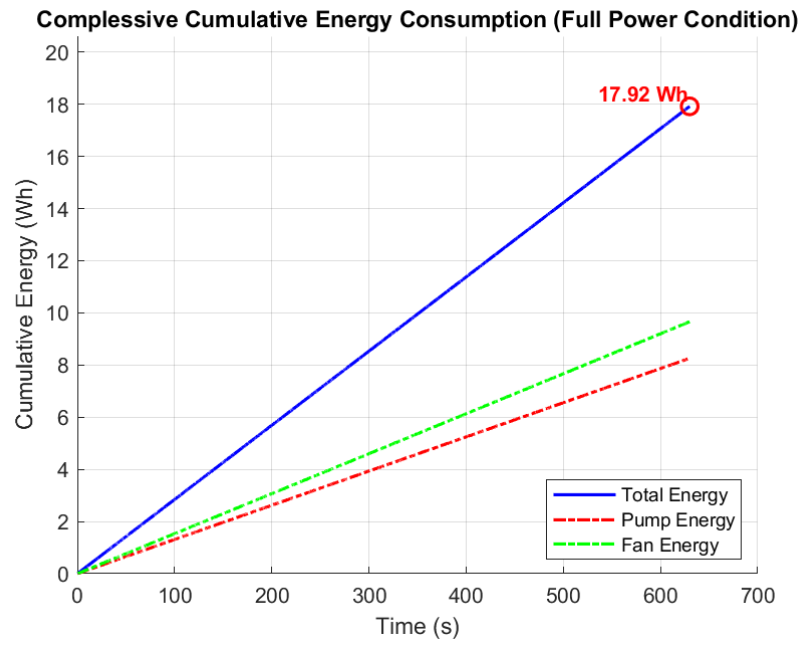


Figure 3.15: Total energy consumption in full power configuration

Optimizing this value will be the objective of the chapter 4.

## Chapter 4

# Control Strategy

In this chapter, a control strategy for the cooling system will be introduced. As anticipated in Chapter 1, a control strategy for the auxiliaries of the cooling system enables the optimization of the LV battery pack sizing by reducing energy consumption. This has benefits in terms of weight reduction and consequently improves the vehicle's dynamics. In the specific field of application, it allows for potential optimization of the score in both static and dynamic events of the competitions.

Control strategies rely on the design and tuning of controllers. For dynamic systems, different types of controllers exist, each distinguished by its characteristics, tuning methods, and performance in various conditions. The selection of a specific controller depends on several parameters, such as system dynamics, response time requirements, robustness, and implementation complexity. In the context of this application, controller selection is crucial to achieving optimal thermal management.

Two different control approaches will be tested. The first one is based on PID controllers, while the second one utilizes an MPC (Model Predictive Control) approach. In the following sections, the advantages and disadvantages of both

control strategies will be explained, and the rationale behind the choice to focus on these controllers will be justified.

The system model will be treated as a plant. The system inputs will be the control variables associated with the fans ( $U_{fan}$ ) and pumps ( $U_{pump}$ ), while the outputs will be the temperature of the EM cooling jacket ( $T_{EM}$ ) and the temperature of the inverter cold plate ( $T_{PM}$ ). These two outputs will be regulated with respect to their corresponding reference temperatures.

## 4.1 Reference Temperatures

The selection of reference temperatures represents a crucial aspect of this discussion. By avoiding excessive cooling of the components, the cooling system can be used less frequently, consequently saving energy. However, it is essential to consider aspects related to the cooling dynamics, carefully evaluating transients at system startup, potential fluctuations in operating conditions, and uncertainties related to sensor measurements.

A possible thermal excursion of ambient temperature between a shaded area and a sunlit area is considered to be 3 degrees Celsius. The uncertainty associated with NTC sensors is estimated to be approximately  $\pm 1$  degree Celsius at a temperature of 60 degrees Celsius.

The de-rating temperature of power modules is set at 70 degrees Celsius [4]. Based on the previous considerations, a target temperature of **63 degrees Celsius** is selected for the outlet temperature of the cold plate. This range provides a safety margin in case of temperature measurement errors and dynamic changes in external conditions, preventing power module de-rating.

Regarding the EM, the maximum nominal operating temperature is set at 80 degrees Celsius. In this case, a reference temperature of **74 degrees Celsius** is chosen, as this component is less sensitive than the power modules and less

affected by thermal variations.

## **4.2 PID**

The PID controller is widely used in the automotive field due to its simplicity, robustness, and effectiveness in a variety of control applications. It is based on three main components: the proportional (P), integral (I), and derivative (D) terms. The proportional term responds to the current error, the integral term accounts for past errors to eliminate steady-state offsets, and the derivative term predicts future errors by considering the rate of change.

PID controllers are particularly suitable for systems where precise regulation and stability are required. Their tuning can be performed through various methods, such as Ziegler-Nichols tuning, trial-and-error adjustments, or optimization algorithms. However, their performance may be affected by system non linearities, delays, and external disturbances, requiring careful parameter selection and sometimes additional compensatory mechanisms.

In the context of cooling system control, PID controllers are often implemented to regulate fan and pump operations, ensuring that the system maintains optimal thermal conditions.

### **4.2.1 Implementation**

The PID controller is inherently a Single-Input Single-Output (SISO) controller, meaning that it is designed to regulate a single output variable based on a single input variable. In this case, two separate variables require control: the variable associated with fan operation and the variable associated with pump operation. Consequently, two distinct PID controllers are implemented.

A fundamental challenge arises due to cross-coupling between the controlled

variables. Cross-coupling refers to the phenomenon in which the system outputs are not independently influenced by their respective inputs. In other words, a change in one input can affect both outputs, creating interactions between the two control loops.

To mitigate this effect, an assumption is made that electric motor temperature ( $T_{EM}$ ) is more strongly influenced by the pump operation. Consequently, the error associated with the EM temperature is used as the input for the PID controller regulating the pumps.

Similarly, the error related to the inverter power module temperature ( $T_{PM}$ ) is used as the input for the PID controller governing the fan. This configuration aims to minimize the undesired interactions between the two control loops while maintaining effective temperature regulation.

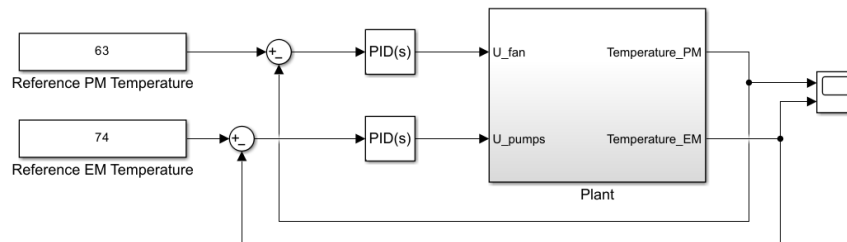


Figure 4.1: Block connection using PID controllers

### 4.2.2 Tuning

For the tuning of the controller, the embedded Simulink tool *PID Tuner* was used. This tool allows for automatic tuning of PID controllers by linearizing the plant and optimizing the proportional, integral, and derivative gains to achieve a desired response. The PID Tuner provides an interactive interface where the closed-loop performance can be adjusted in terms of response speed and robustness.

Before using the PID Tuner, the plant was linearized to ensure that the controller design is based on an accurate model of the system's dynamic behavior. Linearization simplifies the analysis and tuning process by approximating the nonlinear system around an operating point.

The tuning of the first PID is defined by setting the pump power to the maximum and receiving as input the error associated with the temperature at the cold plate outlet. This PID will control the fans.

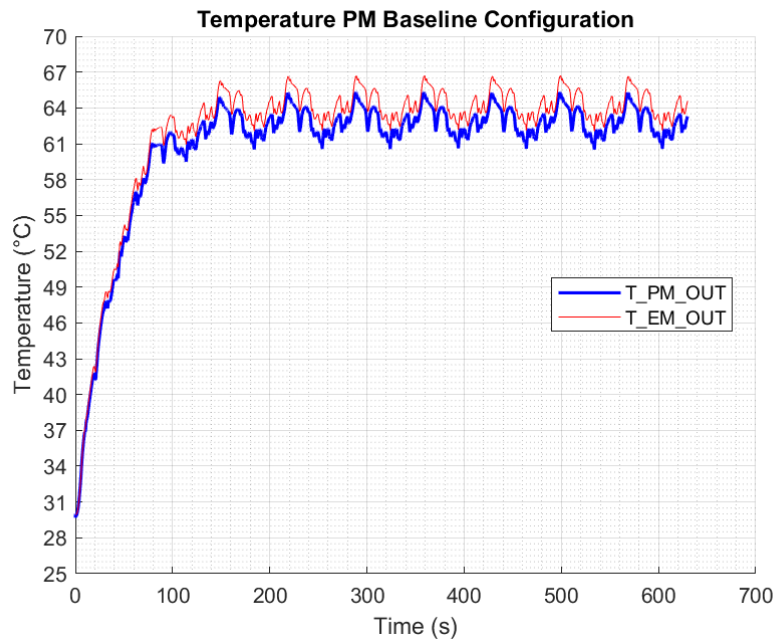


Figure 4.2: Fan PID controller

Figure 4.2 represents the system output when a single PID is applied to the fans to regulate the cold plate outlet temperature to the reference value.

Similarly, for the tuning of the second PID, the fans are set to maximum power. The second PID will act on the pumps and will take as input the error associated with the temperature at the electric motor outlet.

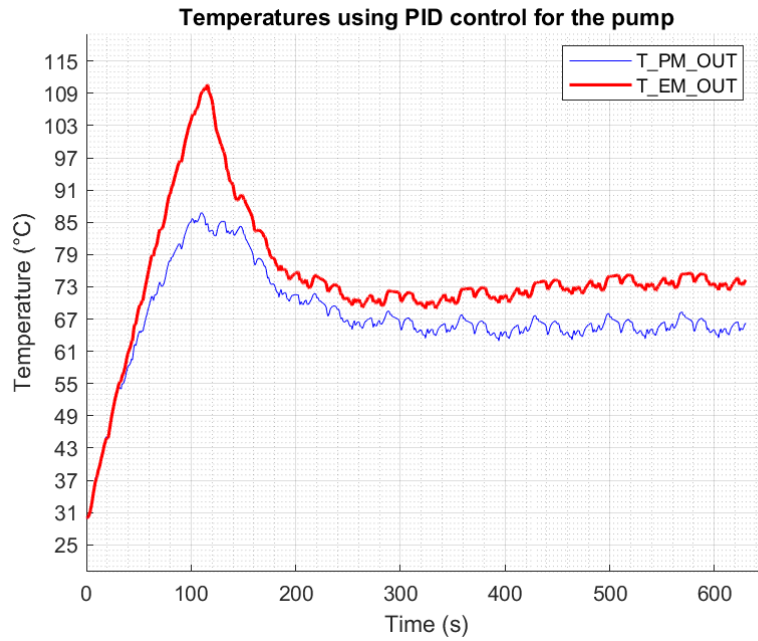


Figure 4.3: Pump PID controller

The obtained parameters for the two PID controllers are summarized in Table 4.1.

Controller	P	I	D	Filter Coefficient (N)
PID 1 (Fan control)	-2.09	-0.0085	-44.04	0.073
PID 2 (Pump control)	-0.31	-0.0039	-1.08	0.088

Table 4.1: PID controller parameters for fan and pump control

### 4.2.3 Outcomes

The following plots illustrate the obtained results.

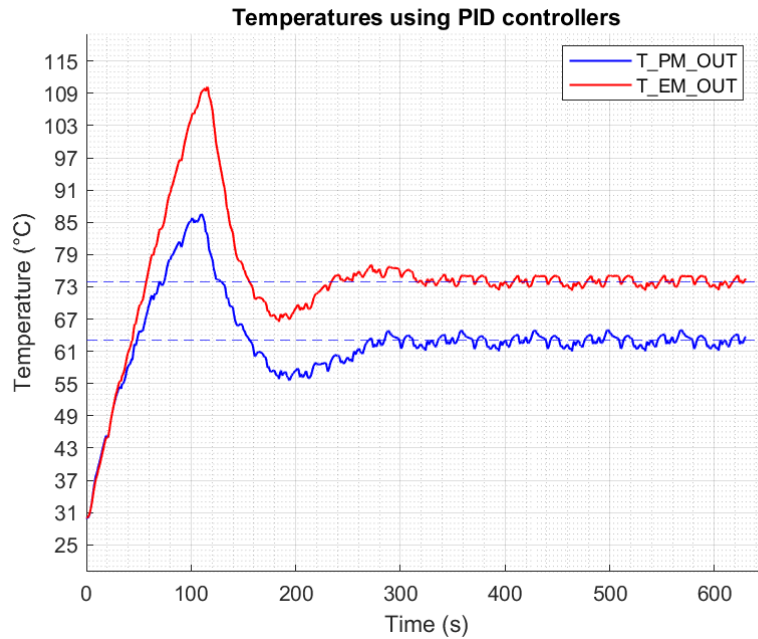


Figure 4.4: Temperature in the cooling loop using PID controllers

The plot shows the outlet temperatures from the cooling jacket and the inverter cold plate. By comparing these values with Figures 3.11 and 3.12, an overall increase in steady-state temperatures can be observed. This result aligns with expectations, considering that under full-power conditions, the system was previously over-cooled.

During the first 300 seconds, a transient response is evident, leading to an overshoot in temperature. This condition is particularly critical for vehicle reliability; however, it is also an expected outcome given the control strategies employed. Despite fine-tuning, it is impossible to completely eliminate the overshoot without sacrificing controller performance. Therefore, this issue will be addressed and resolved implementing a second control strategy to mitigate this effect.

On the other hand, a significant improvement is observed in terms of energy consumption. By activating the auxiliary systems only when needed, a substantial reduction in their energy usage is achieved.

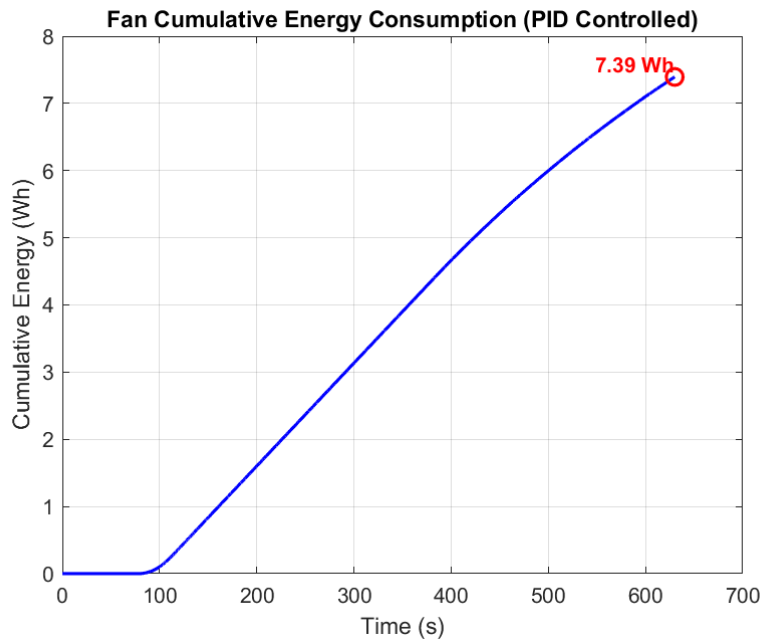


Figure 4.5: Fan energy consumption using PID controllers

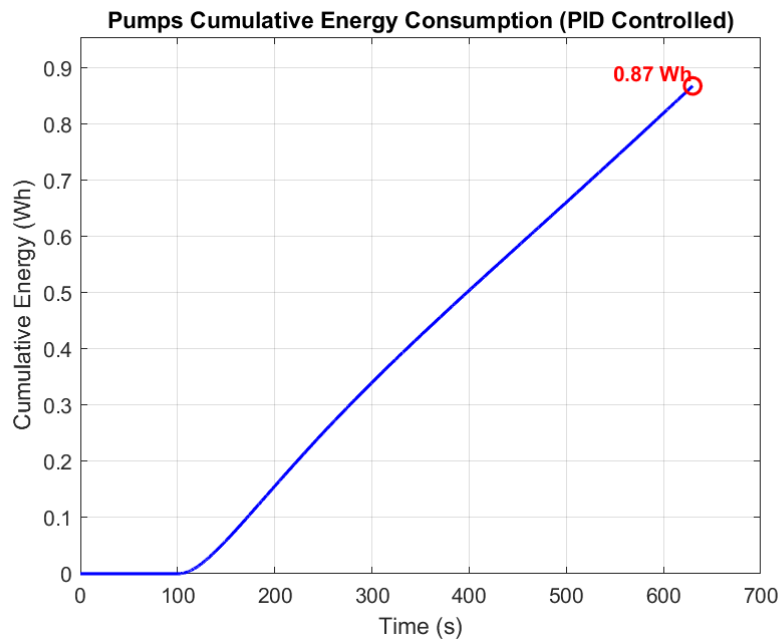


Figure 4.6: Pumps energy consumption using PID controllers

Comparing the total cumulative energy in the case of a controlled system with the graph of the uncontrolled system 3.15, a gain of 53.90% is recorded.

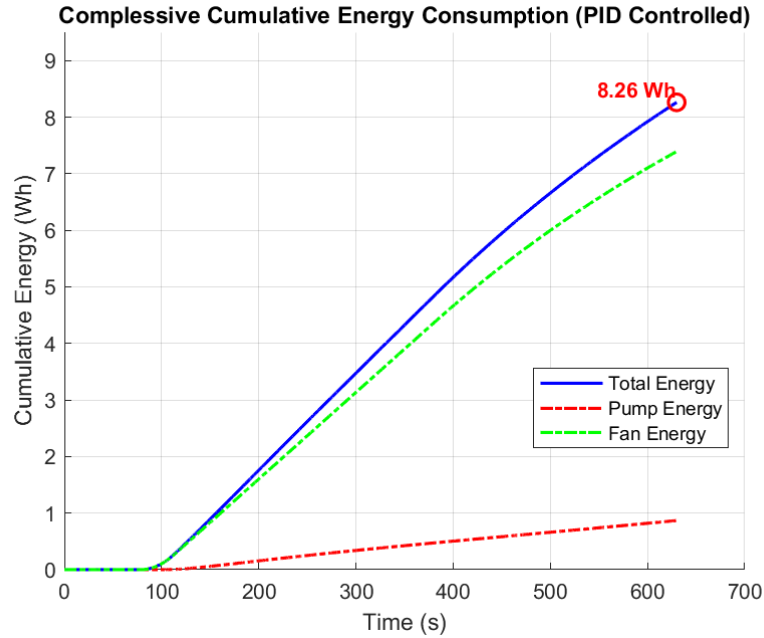


Figure 4.7: Total energy consumption using PID controllers

Comparing the total cumulative energy in the case of a controlled system with the graph of the uncontrolled system 3.15, a gain of 53.90% is recorded.

### 4.3 MPC

Model Predictive Control (MPC) is an advanced control strategy that optimizes system performance by predicting future behavior based on a mathematical model of the plant. MPC incorporates future system dynamics into the control action by continuously solving an optimization problem over a finite prediction horizon. This approach allows the controller to anticipate disturbances and adjust the control inputs proactively, rather than simply reacting to changes as they occur.

One of the key advantages of MPC is its ability to explicitly handle system

constraints. By incorporating physical limitations, such as actuator saturation and operational safety margins, the controller ensures that the system operates within feasible boundaries. Additionally, MPC is particularly well-suited for multi-variable systems, where interactions between different control inputs and outputs must be taken into account. This makes it an effective solution for applications that require coordinated control actions, such as thermal management in automotive cooling systems.

Despite these advantages, MPC also presents certain challenges. The computational complexity associated with solving an optimization problem at each control step requires significant processing power, which may limit its application in real-time systems with stringent timing constraints. Moreover, the effectiveness of the controller heavily depends on the accuracy of the plant model. Any discrepancy between the mathematical representation and the actual system can lead to suboptimal performance, making model identification and validation critical steps in the control design process. Another challenge lies in the tuning process, which is more intricate compared to traditional controllers, as it involves selecting an appropriate prediction horizon, weighting factors, and optimization constraints to balance performance and computational feasibility.

In the context of this study, MPC is evaluated as an alternative to PID control for managing the operation of fans and pumps in the cooling system. The ability to optimize control actions while considering system constraints and interacting variables makes MPC a promising candidate for improving thermal management efficiency. However, its practical implementation requires careful consideration of computational demands and model accuracy to ensure robust and reliable operation.

### 4.3.1 Implementation

Given that the MPC controller is inherently designed for dynamic MIMO (Multiple-Input Multiple-Output) systems, the assumptions previously made to mitigate cross-coupling effects are no longer necessary. Unlike PID control, where separate controllers were assigned to different outputs, MPC can inherently manage the interactions between multiple inputs and outputs within a unified control framework. To facilitate signal processing, the system outputs are grouped into a single signal using the *mux* block. Similarly, the errors associated with each output are also processed collectively, allowing the controller to handle them simultaneously. This configuration enables MPC to optimize control actions while considering the interactions between the fan and pump operations, improving overall system efficiency. For the sake of simplifying the problem, the controller is initially implemented without considering external disturbances. This assumption allows for a more straightforward evaluation of MPC's performance under nominal operating conditions. However, in real-world applications, disturbances could be incorporated into the control model to enhance robustness against unexpected variations in system dynamics. An overview of the block connections used for the MPC implementation is provided in the following diagram.

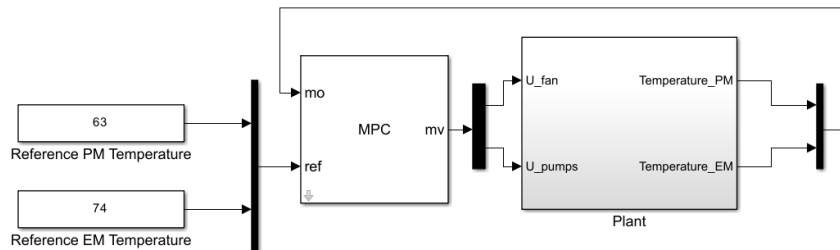


Figure 4.8: Block connection using MPC controller

### **4.3.2 Tuning**

For tuning the MPC block, Simulink provides a dedicated tool. The process begins by designing the controller. After opening the block, the user clicks on the "Design" button, which allows for the definition of the dimensions for both the outputs and inputs. Once these are specified, the model is linearized based on the chosen outputs and inputs. Following these steps, an interface becomes available for tuning the controller parameters. This interface is similar to the one described in 4.2.2, offering a user-friendly environment to adjust and optimize the controller settings.

The Simulink tool for MPC tuning allows users to interactively adjust various control parameters. By linearizing the model based on the selected input and output variables, it provides a simplified yet accurate representation of the system's dynamics. This makes it easier to adjust the controller's settings in a way that ensures optimal performance. The interface allows for fine-tuning of parameters, providing the necessary flexibility to achieve the desired control behavior for the modeled system.

### **4.3.3 Outcomes**

The figure 4.9 show the temperature map obtained.

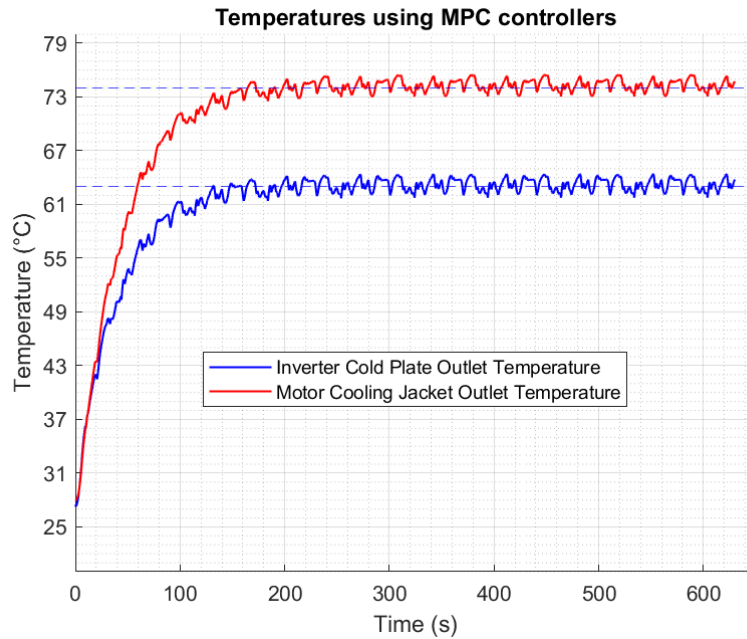


Figure 4.9: Temperature in the cooling loop using MPC controllers

The results demonstrate that the temperatures successfully converge to the reference values. During the transient phase the temperature do not exceed the derating temperature of the components. This ensures the reliability and longevity of the system. The graph highlights the controller's capability to predict the future trend of the dynamic system. By doing so, the MPC controller effectively regulates temperatures, preventing undesired peaks that could lead to component derating. In more severe cases, excessive temperature spikes could result in critical failures, potentially causing system malfunctions or even non-recoverable damage (DNF).

These findings demonstrate the effectiveness of the MPC controller in maintaining stable operating conditions while ensuring system safety and performance. However, it is important to emphasize that the computational power required by this controller during simulation is significant. This factor must be carefully considered when evaluating the feasibility of implementing this control strategy in a

real-world application.

The evaluation of the energy consumption of the cooling system using this control strategy is now being performed. By utilizing equation 3.1 implemented in MATLAB, the cumulative curves associated with the energy consumption of the individual auxiliaries will be plotted.

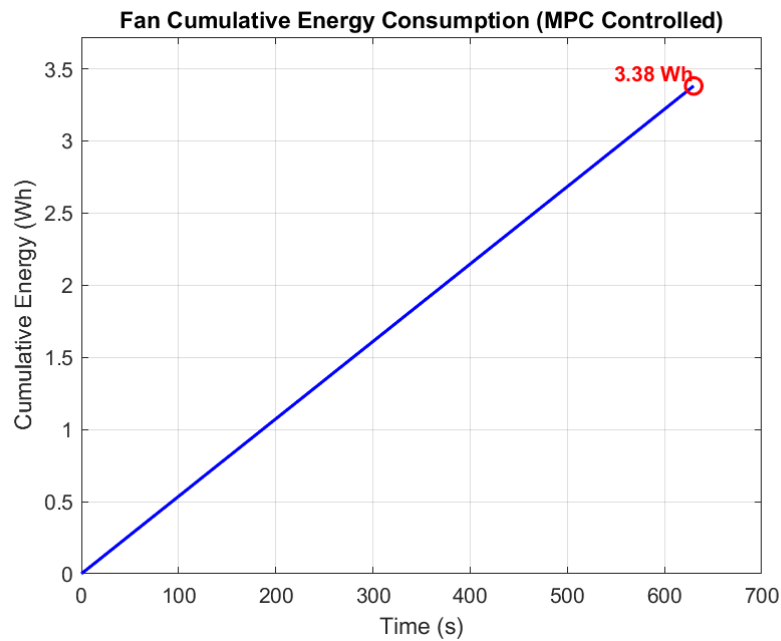


Figure 4.10: Fan energy consumption using MPC controller

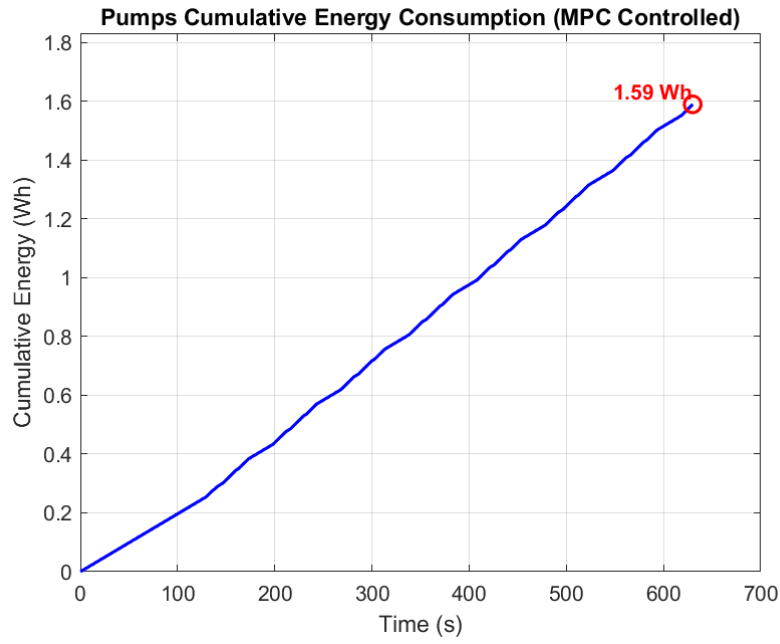


Figure 4.11: Pumps energy consumption using MPC controller

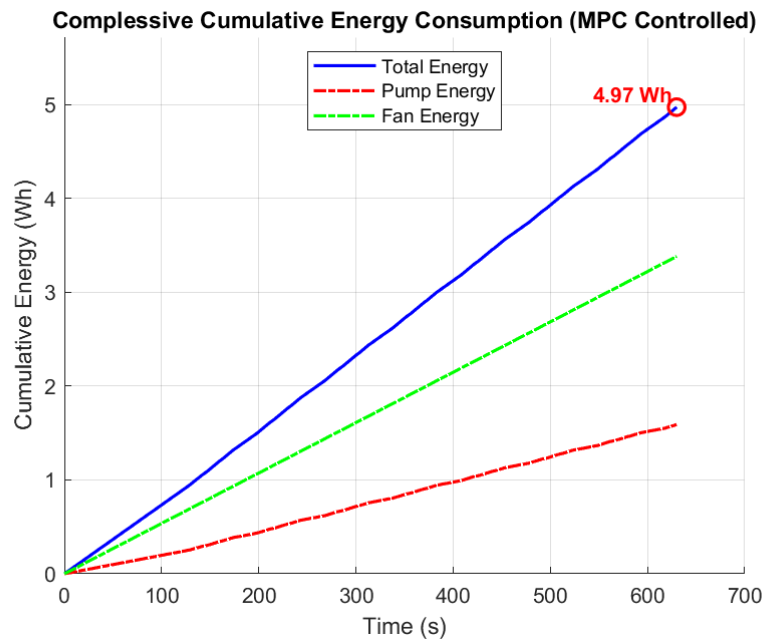


Figure 4.12: Total energy consumption using MPC controller

It can be observed that the energy consumption required by the cooling system undergoes a decrease compared to the full power case. The consumption is reduced by 72.27% in this instance. The results are comparable to the PID case. However, it should be noted that the elimination of the initial overshoot and the speed of convergence to the result are improved. Furthermore, the temperature oscillations appear more robust, with smaller fluctuations than in the PID case.

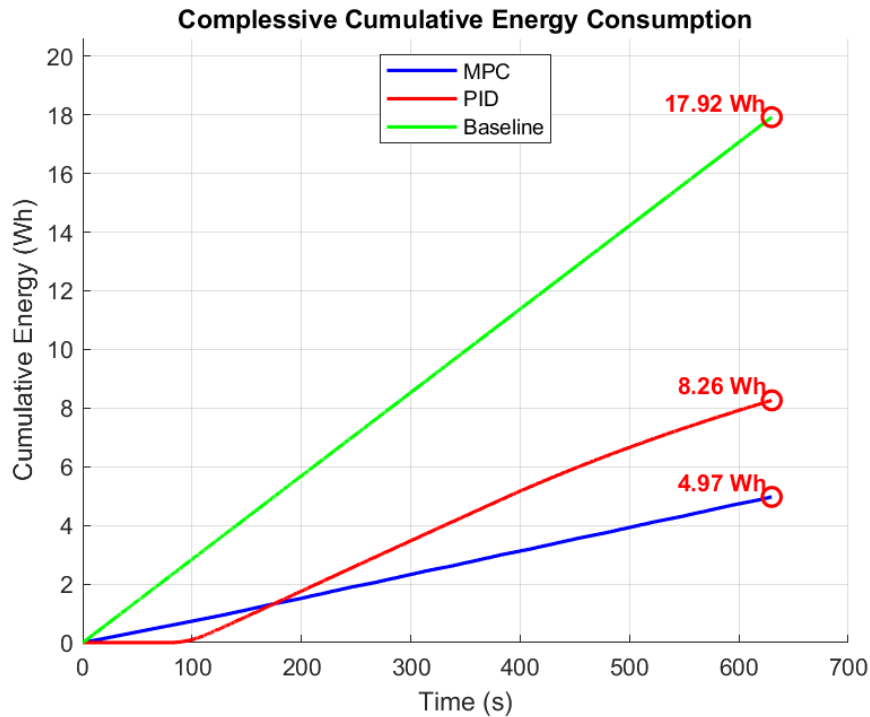


Figure 4.13: Comparison of energy consumption using different control strategy

Figure 4.13 shows a comparison of the different energy consumption results obtained previously. It can be observed that, in the full power case, the cumulative energy consumption is represented by a straight line since there are no power variations over time. It is important to highlight that, during the transient phase, the PID controller has an energy consumption that starts from zero until the observed temperature exceeds the reference value. At that point, its energy

consumption begins to increase more rapidly compared to the MPC controller. The latter, due to its ability to predict possible behaviors within the time horizon, activates the components more gradually, ensuring continuous and smooth cooling.

# Chapter 5

## Conclusions

The implementation of a thermal model represents a fundamental step in gaining an in-depth understanding of and evaluating engineering choices in a cooling system. The thermal model developed for the cooling system of the OUR Formula Student race car provides a suitable balance between level of detail and computational complexity. All available data were incorporated into the model, while missing parameters were reasonably assumed with justified choices. The simulations conducted demonstrate the system's dynamic response, with trends aligning well with both the collected experience in cooling systems and the underlying physical phenomena involved. For future work, it is desirable to obtain experimental data from the cooling system to further validate the model, ensuring a stronger correlation between the simulation and the real-world system.

The integration of a cold plate into the cooling system model was found to be well-suited to the existing framework. Positioning it downstream of the motors aligns with the different operating temperature requirements of the components. The introduction of liquid cooling for the inverters enhances performance by allowing the motors to operate at higher power levels. This methodology is widely recognized in the Formula Student domain and is expected to yield benefits,

including improved performance in static competition events.

Operating the cooling system at full power resulted in excessively low component temperatures, which provided no tangible benefits in terms of vehicle performance. The implementation of a thermal management strategy demonstrated the potential for significant energy savings through the use of controllers for auxiliary system regulation.

The choice of controllers was based on a study of relevant literature and experience in cooling systems for Formula Student applications. The wide range of available control strategies leaves ample room for future studies to determine the most effective control approach. The implementation of PID controllers revealed a significant challenge in tuning them independently. The resulting temperature map exhibited substantial overshoot, which proved difficult to eliminate completely despite extensive tuning efforts. However, the simplicity of PID controllers facilitates their implementation, and their low computational power requirements make them well-suited for deployment on Formula Student vehicle control boards, where computational resources are often limited.

Testing of the MPC controller demonstrated its robustness. Its capability to handle MIMO systems and the ability to impose constraints on control variables and outputs via Simulink's tuning tools allowed for a more refined tuning process. The system showed minimal deviation from reference values, except during the initial transient phase. However, even in this phase, recorded values remained below the derating threshold for both powertrain components.

Energy consumption in both controlled cases was comparable. Once the transient phase was completed, both controllers successfully minimized the error between the temperatures of the electric motor, motor controller, and their respective reference values. The MPC controller proved to be more robust during the initial transient phase, effectively preventing excessive temperature peaks. The

graphs also highlight its predictive capability in adapting to the system's future behavior. Conversely, the PID controller required significantly less computational power, making it easier to run simulations and suggesting greater feasibility for implementation given the computational limitations of the vehicle's control unit.

The recorded energy savings will allow for a potential reduction in the number of battery cells. However, at present, it is not possible to quantify this reduction due to insufficient data on the battery pack and the energy consumption of external components such as electronic control units. Nevertheless, the observed energy savings are substantial. A potential future development involves utilizing the HV battery pack and a DC-DC converter to power the cooling system auxiliaries. In this scenario, the registered energy savings could also contribute to the efficiency scoring in the static competition events.

# Bibliography

- [1] Davies Craig. *EBP series datasheet*. 2020.
- [2] San Ace. *140 9RA DC fan datasheet*. 2020.
- [3] Plettenburg. *Operating Manual Industrial Motors Nova-15 (Rev. 1)*. Apr. 2016.
- [4] Plettenburg. *Operational Manual Plettenberg Motor Control MST-140-200 (Rev. 8.1)*. 2023.
- [5] Dimitar Ruzhev. “Design, Build and Test of Prototype Motor Controller for a Single Seat Electric Race Car”. MA thesis. Department of Engineering Science, University of Oxford, May 2021.
- [6] Kader A. Fellague, S. “Huey” Hu, and Donald A. Willoughby. “Determination of the Effects of Inlet Air Velocity and Temperature Distributions on the Performance of an Automotive Radiator”. In: *SAE Technical Paper 940771* (1994). DOI: [10.4271/940771](https://doi.org/10.4271/940771). URL: <https://doi.org/10.4271/940771>.
- [7] Kamal Rawat Prabhakar Bhandari Robin Kumar Thapa Vijay Singh Bisht. “Computational Analysis of Automobile Radiator Roughened with Rib Roughness”. In: *Journal of Heat and Mass Transfer Research* (2022). DOI: [10.22075/jhmtr.2023.27617.1382](https://doi.org/10.22075/jhmtr.2023.27617.1382).

- [8] Alexander Anthon; Zhe Zhang; Michael A. E. Andersen; Donald Grahame Holmes; Brendan McGrath; Carlos Alberto Teixeira. “Comparative Evaluation of the Loss and Thermal Performance of Advanced Three-Level Inverter Topologies”. In: (). DOI: [10.1109/TIA.2016.2639462](https://doi.org/10.1109/TIA.2016.2639462).
- [9] Benjamin Campbell. “Design, Build and Test of Prototype Motor Controller for a Single Seat Electric Race Car”. MA thesis. Department of Engineering Science, University of Oxford, May 2021.
- [10] Frank M. White. *Fluid Mechanics*. 8th. McGraw-Hill Education, 2016.
- [11] David A. Staton and Andrea Cavagnino. “Convection Heat Transfer and Flow Calculations Suitable for Electric Machines Thermal Models”. In: *IEEE Transactions on Industrial Electronics* 55.10 (2008), pp. 3509–3516. DOI: [10.1109/TIE.2008.927000](https://doi.org/10.1109/TIE.2008.927000).
- [12] Formula Student. *Formula Student Rules 2024, Version: 1.0, Rev-ba690a0*. 2024. URL: <https://www.formulastudent.de>.